NTNU – Trondheim
Norwegian University of
Science and Technology

Numerical Investigation of the Hemodynamics in the Human Fetal Umbilical Vein/ Ductus Venosus Bifurcation

Elisabeth Meland

Master of Science in Mechanical Engineering
Submission date: July 2012
Supervisor: Leif Rune Hellevik, KT

Norwegian University of Science and Technology
Department of Structural Engineering

Preface

This report is a result of my Master thesis at The Norwegian University of Science and Technology, Department of Applied Mechanics.
The thesis focuses on the fetal circulation in context of several diseases.

Performing simulations based on my learning through this study have led to an improved knowledge concerning this topic. Combining theoretical and experimental work provide this thesis an overall interesting and motivating structure. The work has had a duration of 21 weeks, and represents a study load of 30 ECTS credits.

I would like to express a special thanks to my supervisor Leif Rune Hellevik, for guidance and help throughout this thesis, and Phd. candidate Paul Roger Leinan for assistance regarding his code that has been used in this study. I would also like to thank Vinzenz Eck for assistance regarding the vascular Polychaos.

Abstract

The transport of oxygenated blood from the placenta to the human fetus has received great attention in clinical Doppler velocimetry studies, especially the ductus venosus. The ductus venosus is connecting the intra abdominal portion of the umbilical vein and the inferior vena cava at the inlet of the right atrium and is therefore significant when examining the fetus state of health. In this thesis, the distribution and pulsations of flow waves in the ductus venosus, umbilical vein and left portal vein are investigated. Furthermore, important model parameters of the fetus circulation are determined with stochastic simulations and sensitivity analysis. The sensitivity analysis was put forward in order to interpret the uncertainty of the many variables in the fetus circulation and how the flow waves are affected. The deterministic blood flow was modelled with a 1D mathematical model. A combination of the 1D mathematical model with a generalized Polynomial Chaos method was applied for the stochastic simulations. All the simulations in this thesis are performed in context of fetal diseases, motivated by typical detrimental signs in fluid mechanics related to the umbilical vein/ductus venosus bifurcation. Furthermore, reversed flow in ductus venosus during atrial contraction, often observed in chromosomally abnormal fetuses was demonstrated. It was found that the reason was high pressure difference between ductus venosus and left portal vein. Pulsations transmitted into the umbilical vein is another detrimental sign in fetus circulation and the parameter providing such pulsations is the diameter of ductus venosus. Further investigations related to the model parameters as well as boundary conditions are suggested in order to expand knowledge and confidence establishing the fetus well being.

Sammendrag

Transport av oksygenrikt blod fra livmoren og inn til fosteret har fått stor oppmerksomhet, spesielt ductus venosus. Ductus venosus er bindeleddet mellom den intra abdominale delen av navlestrengen og inferior vena cava ved innløpet høyre atrium. Dette gjør at ductus venosus er av betydelig verdiful ved unders okelser av fosterets helse. I denne oppgaven er volum og trykk bølgefordelingen i ductus venosus, navlestrengen og *left portal vein* undersøkt. Videre er viktige modell parametere av foster sirkulasjonen bestemt ved hjelp av stokastiske simuleringer og sensitivitetsanalyse. Sensitivitetsanalysen er gjort for åtolke usikkerheten av de mange variabler i fostersirkulasjonen og hvordan bølgeforplantingene blir påvirket. De deterministiske simuleringene ble modellert med en 1D matematisk modell. En kombinasjon av den 1D matematisk modellen og en generalisert Polynomial Chaos metode ble brukt for de stokastiske simuleringene. Alle simuleringene i denne oppgaven er utført i sammenheng med sykdommer som kan oppstå under svangerskapet. Den reverserte strømningen som kan oppståi ductus venosus ved kontraksjon av hjertets atrium, ofte observert i et foster med en kromosomfeil, er blitt demonstrert. Det ble funnet at årsaken til dette var en høy trykkforskjell mellom ductus venosus og *left portal vein*. Pulseringer i navlestrengen er et annet uheldig tegn på foster komplikasjoner. Det ble vist at diameteren til ductus venosus er hovedårsaken til slike pulseringer.

Assignment

In this thesis, a numerical investigation of the hemodynamics in the human fetal umbilical vein/ductus venosus bifurcation will be conducted. How the flow pulsations in the ductus venosus affect the umbilical flow pattern will be of interest. In addition, the flow distribution into left portal vein and the ductus venosus will be examined. Several diseases will be presented and discussed in relationship with the pulsations in flow and the degree of shunting though ductus venosus and left portal vein. Furthermore, a sensitivity analysis is established where several uncertain parameters are simulated and their influence and effect on flow waves examined. The simulations are performed with a 1D model.

Contents

List of Tables

List of Figures

Nomenclature

Δt	time step
δx	length of a vessel segment
Δx	distance between two gridnodes
T	Total time of simulation
λ_1	speed of w_1
λ_2	speed of w_2
λ_w	wavelength
Λ	eigenvalue matrix
$\mathcal{M}$	system matrix
$\mathcal{R}$	right eigenmatrix
μ	dynamic viscosity of blood
ρ	blood density
$\tilde{c}$	Fourier coefficient of the polynomial chaos expansion
C	vessel compliance
c	pulse wave velocity
E	Young modulus
h	Wall thickness
N	Number of grid nodes
Q_f	Forward contribution of Q
Q_b	Backward contribution of Q
r	vessel radius
D	vessel diameter
STD	standard deviation
t	time
$\mathbf{u}$	vector of primary variables; P,Q and A
v_z	mean axial velocity
w_1	forward Riemann invariant
w_2	backward Riemann invariant
$z = (z_1, ..., z_D)$	D-variant random vector containing random variables
Z_c	characteristic impedance
z_i	continuous random variable

1 Motivation

It must be stated that this is a study regarding the fetus affected by a disease, however, rather than only focus on discovering the disease, future research into this particular field may bring along knowledge supporting medical techniques towards a healthy fetus. Today, it is a trend to seek an abortion if the fetus have a disease discovered at an early stage of gestation. Therefore, increased knowledge regarding the reason for the various diseases is necessary in order to prevent it if possible. The only choice may not be an abortion, but a medical way to make the fetus healthy, or provide necessary follow up after birth if for instance cardiac malformation is present. Accordingly, mathematical models may help to understand fetal physiology and pathology, with potentials for improving fetal heath.

2 Introduction

The fetal liver, umbilical and portal veins, ductus venosus and hepatic veins, and the inferior vena cava (IVC) are the main area of interest in the examination of venous blood return to the heart of the fetus [25]. This subject will be focused in this current study. The ductus venosus (DV) has a significant function in the return of venous blood, where it shunts well-oxygenated blood directly towards the right ventricle of the heart through the IVC. The amount is however under discussion where different volumes represent various conditions. Several pathological circumstances are related to the material and fluid behaviour of the ductus venosus where the degree of shunting as well as reversed flow waves are interpreted as negative signs. In addition, the DV acts as transmission line in the opposite direction for the atrial pressure waves [29]. Furthermore, the shape, viscosity, compliance, and in particular the diameter of the inlet are suggested to affect the pulsations of the blood flow in DV, and determine to what extent the degree of waves transmitted into the umbilical vein. However, not only are the pulsations dependent on the characteristics of DV, but also the size and compliance of the umbilical vein itself. Moreover, pulsations after the first trimester in the umbilical vein are understood as detrimental [29]. Recognisable waves during atrial contraction may only be transmitted into the umbilical vein with a patent ductus venosus, yet under normal conditions a major part of the pulse wave is reflected at the junction between the ductus venosus and umbilical vein. Therefore, visible pulsations are rarely discovered in a normally compliant umbilical vein. However, this is in contrast to the left portal vein, which is only a fraction away [33]. Nevertheless, it is the pulsations occurring in the umbilical vein that is in focus in this thesis. Wave transmission and reflection phenomena in the UV/DV bifurcation require an increasing knowledge in order to interpret the pulsatile changes discovered during fetal diseases. Furthermore, once information regarding the mechanical properties of the UV and DV is accessible, the wave propagation can be established in a mathematical model, providing a more meaningful interpretation of considerable clinical findings [17]. furthermore, the investigation into the foetal circulation is related to many uncertainties, such as boundary conditions as well as various material and fluid parameters. The true physics of the human fetal circulation is extremely complex, i.e., large variability in fetal condition and its naturally non-linear behaviour. Consequently, the need to investigate the sensitivity of uncertain parameters are valuable in detecting the cause of incorrect behaviour related to the fetus circulation. Therefore, a sensitivity analysis will be established in this current study, enhancing knowledge regarding which parameter that influences the flow pattern considerably.

In this thesis, several fetal diseases will be presented and related to representative signs of fluid mechanics. The mechanism of redistribution and pulsations of blood flow between the left portal vein, ductus venosus and the intra abdominal portion of the umbilical vein will be discussed. A sensitivity analysis will be established and discussed in context of

important parameters that strongly influence the flow pattern, especially in the ductus venosus and umbilical vein. Both deterministic and stochastic simulations will be utilized.

2.1 Theory

2.1.1 The Fetal Circulation

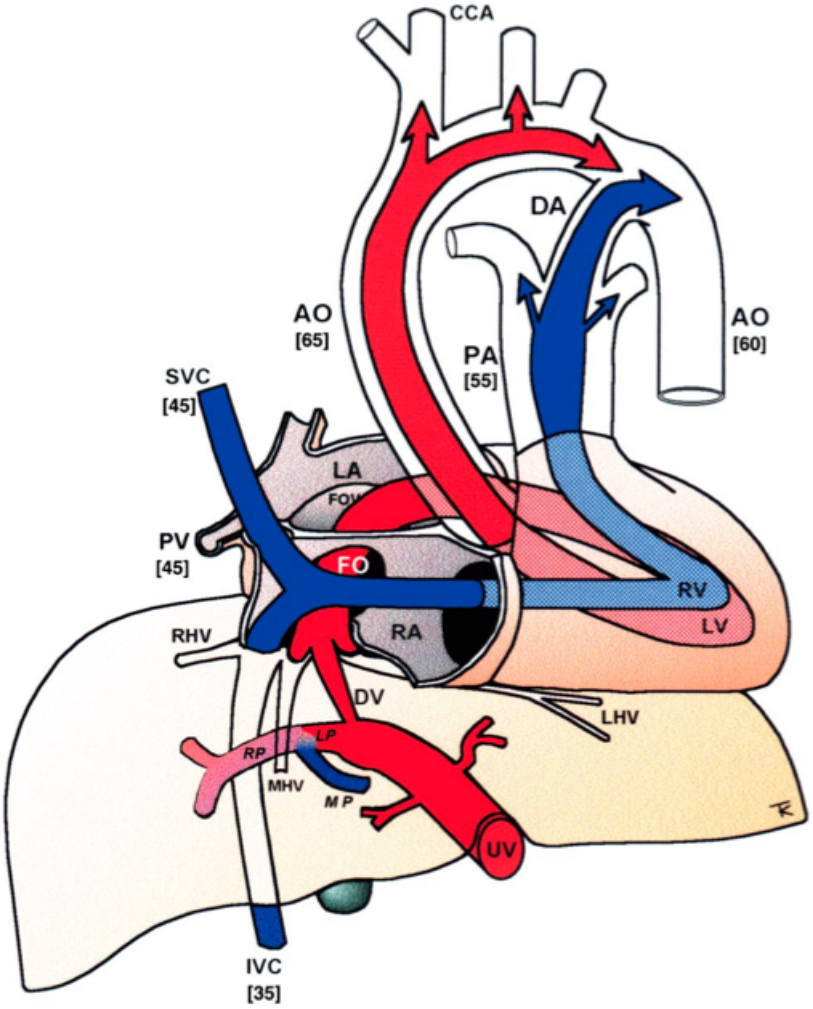

Figure 1: The fetal circulation, demonstrating the blood flow directions and the locations of blood vessels . Taken from Kiserud T. [32]

The physiological position of the DV in the circulation, and its extraordinary hemodynamic properties and regulatory mechanisms make the tiny DV different from all other venous sections, carrying the potential of unique diagnostic information Torvid Kiserud.

The velocity pattern in the ductus venosus is an immediate reflection of the cardiac function, which highly put forward the fact that this vessel is extremely important in the foetal circulation providing information regarding the foetal well-being [31].

The behaviour of DV is an "arterialized" vessel with high pulsatile flow and forward velocities throughout the whole cardiac cycle. For this reason, DV attend to be the most beneficial vessel when it comes to indirectly determining the cardiacs condition.
The vessel acts as a transmission line towards the umbilical vein for pulse waves created

in the heart carrying important information about the cardiac function that are mainly determined by local variation in impedance and compliance [30].

Ductus Venosus (DV) is the main connection of blood from the placenta transporting well-oxygenated and nutrient-rich umbilical venous blood to the brain and myocardium [3]. The DV is trumpet shaped with a narrow inlet (isthmus) measured to be 0.5 mm at mid-gestation and to further increase to a value at about 2 mm at late gestation. The outlet diameter is about 1.25 to 3 mm during the same period. The length of the DV is measured to be 20 mm at term [23].

As the blood leaves the umbilical vein and enters the ductus venosus, the blood velocity increases enormously and represents the highest blood velocity in the venous system. Moreover, the velocity profile has after mathematical computer simulations and animal experiments demonstrated to be a rather partially blunted having a mean/maximum velocity ratio equal to 0.7, and it is claimed that this essentially remains constant [30]. This is illustrated in figure 2 and 3

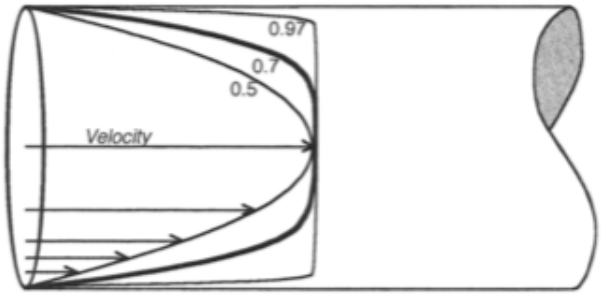

Figure 2: Various velocity profiles in a blood vessel, where the ductus venosus represent profile numbered as 0.7. Illustration taken from Kiserud [30]

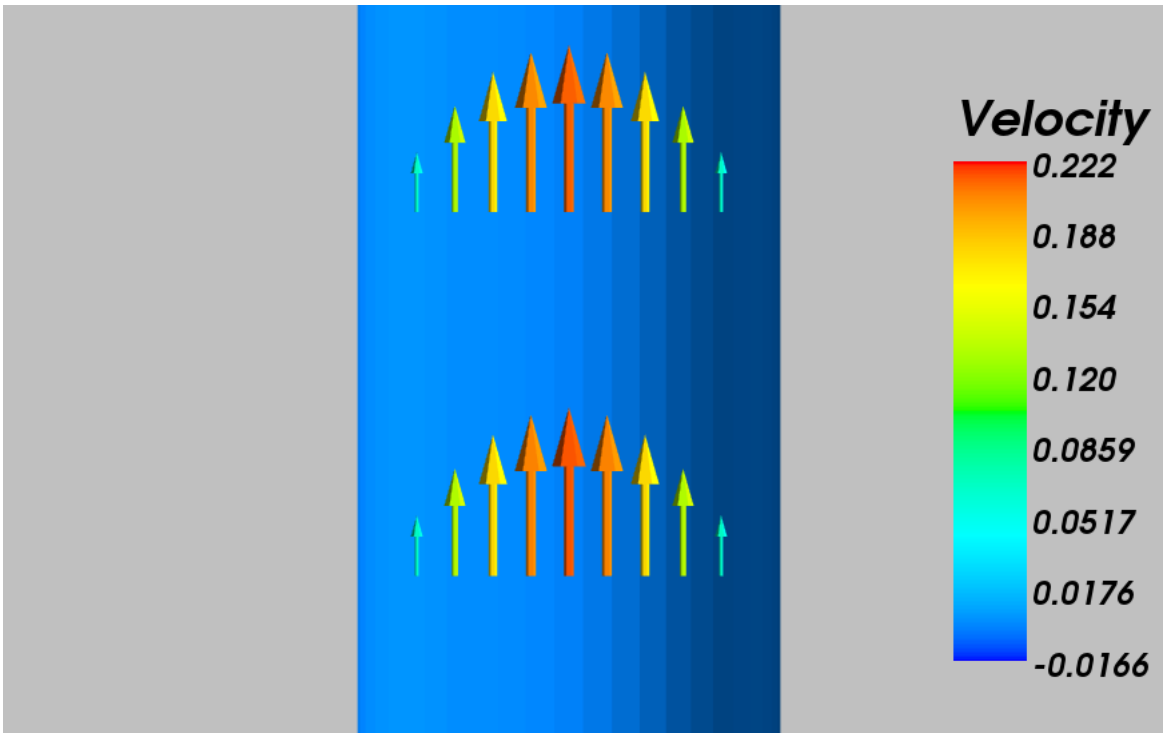

Figure 3: velocity profile in the umbilical vein

The amount transmitted into the UV can be estimated by changes in the impedance, particularly by reflecting mechanisms. The (Z_{dv}) and (Z_{uv}) represent the impedance of ductus venosus and umbilical vein respectively. The reflection coefficient (R_{dv-uv}) can be expressed by means of the two impedances and establish the degree of reflection as well as the pulse wave transmitted at the junction. The reflection coefficient is given by:

$$R = \frac{Z_{uv} - Z_{dv}}{Z_{uv} + Z_{dv}} \tag{1}$$

Moreover, the cross sections of the blood vessels are the single most important parameter of the impedance. As a result, the relatively high difference between the ductus venosus and umbilical vein forces most of the pulse wave to be reflected, and only a minor transmitted into the umbilical vein. This phenomenon supports the fact that pulsations in the umbilical vein do not occur under normal conditions. However, pulsations do occur during the first trimester of gestation, explained by the small dimensions of the vessels.

An important aspect in foetal circulation is the passive regulation of viscosity and pressure in fluid dynamics. The blood has Newtonian properties with low viscosity in the ductus venosus. In the liver tissue on the other side, non-Newtonian properties is present in addition to low blood velocity and high viscosity, hence, resistance [32]. The amount of haematocrit, has an effect on the viscous resistance in the low velocity venous liver flow and little influence in the ductus venosus where higher velocities are present. Therefore, due to the haematocrit, the umbilical venous flow shifts from the liver to the ductus venosus. [32]. It must be stated that this will not be demonstrated by simulations due to limitations of the 1D model.

2.1.2 Acting as a Sphincter

It has been suggested that the ductus venosus inlet was in control of the degree of shunting by means of a "sphincter". This blood vessel seemed to be under adrenergic control with the ability to expand in order to regulate the portion of oxygen [30]. Nevertheless, it must be stated that only anatomic findings is related to animals. Determination of a muscular activity in the human foetus is quite controversial due to lack of anatomic evidence and also *in vivo* observations of diameter dilatation [20]. Furthermore, the entire length have been suggested to operate as an active regulation, and not only the inlet [31]. This mechanism will not be investigated directly, but several measurements including an expanding of the ductus venosus diameter will be elaborated.

2.1.3 First Half of Pregnancy

The velocity is estimated to be 50 cm/s during early pregnancy (10 to 15 weeks gestation) [30] The degree of shunting though the ductus venosus 20 % to 30 % at mid gestation and remains the same throughout the pregnancy, however, other volume flow have been published.. ref ref ref!

The shunting through ductus venosus is probably of higher relevance during the first trimester than at term. In particular, the reversed blood flow occurring at atrial contraction is thought to be the most important signal and is often related to various diseases such as chromosomal abnormalities and cardiac malformations (between 10-14 weeks of gestation) [30]. However, at 15 weeks of gestation a negative velocity during atrial contraction may be present. Furthermore, zero velocities may include both negative and positive velocity directions. Thus, a test in order to clarify such pulsations related to pathological conditions is in need. Wave splitting results in knowledge of such flow and has therefore been applied later on in this thesis. Wave splitting theory is elaborated in section 3.3.1.

2.1.4 Second Half of Pregnancy

It has been argued that the shunting through the ductus venosus is more important at the early stage of pregnancy and the degree of importance vanishes after 30 weeks [32]. It is further assumed that the degree of shunting prioritise the liver where approximately 80% is transmitted at the last part of pregnancy. Nevertheless, in an hypoxic condition, the priority is argued to be different and the ductus venosus is preferred aiming for a sufficient amount of oxygen delivered to the heart as well as the brain [32]. If such a challenge occurs, the development of the liver may be affected. The velocity is about 65 cm/s near term [30].

Simulations with the aim of reasons why flow prioritise one vessel or the other is presented in table 4 and 5, whereas the geometry, wall thickness and young modulus have been in focus. The young modulus represents the stiffness of the blood vessel.

2.1.5 Blood Flow Waveforms

Typical waveforms in the blood vessel include three phases. The highest pressure gradient between the venous vessels and the right atrium is present at the time of ventricular systole. Hence, maximum blood flow velocities towards the fetal heart takes place at that part of the cardiac cycle. Furthermore, during early diastole, a second peak take place. The nadir of the flow velocities occurs during atrial contraction in late diastole [25]. This is illustrated in figure 4

Under normal circumstances, the blood flow in the ductus venosus does not tend to zero during second half of pregnancy. Nevertheless, it might reach zero or below before 15 weeks of gestation [29]. Under pathological circumstances, below zero velocities may be present and it is the wave during atrial contraction that has been estimated to provide information regarding the state of health.

In should be stated that not only is a pathological condition the reason for an abnormal waveform, but also local changes such as the foetal position. For instance, a foetus bending forward may squeeze the IVC, and the outlet or the entire length of the ductus venosus may result in an almost total reflected wave and no pulsations. Yet, this is only observed in 3% of pregnancies, and it is usually re-established after a few minutes due to foetal movement back into position. Nevertheless, a normal ductus venosus does not exclude abnormal physiology. All the factors that influence the flow pattern should be taken into consideration. An example to this is when no abnormal waveform is observed in the ductus venosus, when in fact, the myocardium is ill conditioned. The myocardium may itself compensate for the increased stiffness of the muscle by increasing the cardiac volume, hence, increasing the compliance. If this is the case, then no abnormal flow will be observed, and a decision regarding the state of health my be incorrect [31]. On that account, the importance of significant knowledge concerning the fluid dynamics as well as material mechanics is certainly valuable insuring against incorrect decision of the state of health. Furthermore, not only are the presence of disease valuable to discover during pregnancy, but also for continuous observation in later life. A cardiac malformation during gestation may be present after birth.

2.1.6 The Atrial Contraction Wave

From a diagnostic point of view the atrial contraction wave in the ductus vensous is the single most important wave of the waveforms. This wave support information regarding the end diastolic filling pressure. An augmented atrial contraction wave implies an increased end-diastolic filling pressure in the heart, that may have been caused by an increased distension of the atria which tend to an increased contraction (the Frank-Starling effect), [31]. This happening is often observed in congestive heart failure, see section 3 for enhanced discussion. Simulations related to such a wave will be conducted, investigating the cause of an abnormal pulse wave occurring in the ductus venosus.

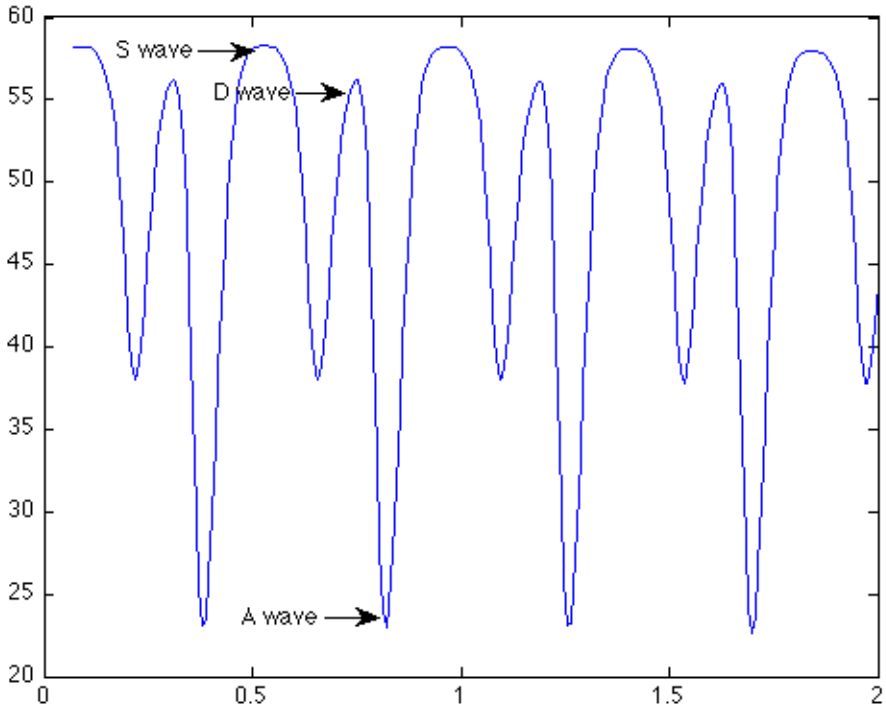

Figure 4: The different waves occuring during a cardiac cycle in ductus venosus

3 Fetal Diseases

Hechet et al. [25] have presented a study on the venous blood flow related to fetal diseases. The occurrence of pulsations in the umbilical vein during atrial contraction has been put forward as an unfavourable indication of a pathological condition. Due to the direct connection between the ductus venosus and the umbilical vein, abnormal flow in the ductus venosus may also be interesting to investigate due to the propagating wave originated by the fetal heart through the IVC, entering the ductus venosus and towards the umbilical vein. Abnormal pulsations in this particularly region are associated with a numerous diseases where some of them will be presented in this thesis. To illustrate the extent, as much as 64 % of the fetuses affected by absent end-diastolic velocities within the umbilical artery or non-immune hydrops died if pulsations in the umbilical vein were present. In comparison, 7 % died if the pulsations in the umbilical vein did not exist. In addition, pulsations in the umbilical vein when an increase of reversed flow during atrial contraction occurs in the IVC, hence also in ductus venosus, has been suggested as an incorrect cardiac function.

3.0.7 Chromosomal Abnormalities

In 1997, a pioneering work demonstrated that a numerous of fetuses with trisomy 21 among other chromosomal abnormalities had abnormal flow in the DV at 11 to 13 weeks of gestation [23]. The reason for an abnormal a-wave in DV which is associated with trisomy 21 is not entirely established. Nevertheless, it is considered to be due to the performance of the fetal cardiac. During the first trimester, the cardiac has a stiffer and less compliant structural and functional condition which supports this reversed a-wave. Thus, from a mechanical point of view, the a-wave reversal may be explained by the atrial wall, contracting against a relatively stiffer wall resulting in an increased back pressure. Therefore, the blood flow may either be stopped or reversed during atrial systole.

In a study by Matias et al. [12] reversed or absent flow during atrial contraction was detected in the ductus venosus. However, abnormal flow in this vessel was also discovered in 3.1 % of the chromosomally normal fetuses. Furtermore, in comparison with the normal group , not affected by chromosomal abnormalities, it was observed that the median amplitude of the s-and d- waves were notably lower. In addition, the pulsatile index(PIV) was much higher. Nevertheless, a regression analysis showed that it was the a- wave that was a clear factor separating the chromosomally abnormal and normal fetuses.

3.0.8 Cardiac Defects

Congenital heart defects (CHD) are the greatest widespread defect and the cause of 20% of spontaneous abortions, 10% of stillbirths and 1% of term pregnancies. Furthermore, cardiac defects are responsible of over 50% of deaths where the child had a defect present at birth [23]. In a study by Maiz et al. [11] it was stated that the risk of a cardiac defect is three times the chance if there exist an abnormal flow in DV, and halved if normal flow was present. As a result, a suggestion has been made that abnormal flow in DV during the first trimester could be a predictor of CHD [23].

3.0.9 Hypoxia

Hypoxia is compulsory for fetal development,nevertheless, excessive hypoxia provide lasting negative consequences. Complications due to fetal hypoxia are among top 10 causes of fetal death [6]. Factors such as hypertension, anemia, pulmonary disease, drug abuse and smoking caused by mother may contribute to fetal hypoxia. Moreover, hypoxia may result in intrauterine growth restriction (IUGR) and low birth weight and is related with prematurity, infant mortality and an increasing risk of adult cardiovascular disease [6]. As already mentioned, detecting cardiovascular disease during fetal life is indeed important, not only in order to make decision at that time, but also to provide significant follow up in later life.

It has been suggested that hypoxia preferentially compromises early heart development. Ream et al. [6] proposes that hypoxia compromise the fetus through myocardial hypoplasia (underdevelopment of an organ or tissue) and reduction in heart rate. Prolonged hypoxia results in a thin and disorganized ventricular myocardium, and will affect the cardiac output.

The laplace equation is given by

$$\sigma = \frac{Pr}{t} \tag{2}$$

where t is the wall thickness, σ wall stress and P the ventricular pressure.

A reduced ventricular wall thickness will have an impact on the pressure, whereas a reduced wall thickness will result in a reduction of pressure in order to compensate the wall stress [14]. It is therefore likely to believe that a reduction in pressure originated from the heart will affect the volume flow in the umbilical, left portal vein and ductus venosus bifurcation. It has been demonstrated that low pressure at the IVC compartment, provide a higher flow shunted through the ductus venosus. In contrast, a high pressure at the IVC compartment will result in a reversed flow at the ductus venosus.

Tchirikova et al. [10] states that a consequence related to hypoxia is an increase in the shunting through DV. It is most likely due to the importance of a significant amount of oxygen and glucose to the brain as well as the heart. In support, an animal study showed that during induced hypoxia or reduced umbilical blood flow, the umbilical shunting

though the DV was increased. In addition, an active ductal dilation was put forward as a hypothesis in order to sustain this hemodynamic adjustment. Such an adjustment is enhanced in section 2.1.2.

3.0.10 Growth-Restricted Human Fetuses

Small for gestation (SGA) and intrauterine growth restriction (IUGR) are often used to describe the small fetuses. SGA was introduced in 1967 by neonatologists in order to categorize the newborns with a birth weight less than the 10th percentile. Furthermore, SGA became a widely used expression classifying the under grown fetuses despite the cause of a specific disease. Terms such as SGA, fetal growth restriction and IUGR are often used, yet the term IUGR will be used in this thesis because it reflects the condition of the fetus as well as the placenta [22]. It must be stated that 70% of fetuses with a fetal weight of less than 10th percentile are small for normal reasons, and accordingly not at risk. However, 30 % are pathologically small with the consequence of numerous complications, and worst case fetal death [22].

Bellotti et al. [7] have studied the blood flow in a large series of growth-restricted human fetuses. The purpose of this study was to evaluate the changes in the distribution of blood flow from the umbilical vein towards the liver and ductus venosus in intrauterine growth-restricted human fetuses together with the dilation of the ductal isthmic diameter (The dilation of the ductus venosus has not been taken into consideration in this thesis due to 1D modelling complications). The degree of shunting though ductus venosus is increased in fetuses affected by IUGR. In comparison, the percentage of blood flow towards the right lobe showed a considerable reduction. It was observed that a combination of a reduced umbilical venous blood flow and an increased ductal shunt may adjust the perfusion of the fetal liver.

Moreover, it has been indicated that for IUGR fetuses, the blood flow through the DV towards the vital organs (brain and myocardium) remains the same within the normal ranges for gestational age (33.3 % 18.1 mL/min in normal fetuses; 40.3 % 19.4 mL/min in IUGR fetuses). Accordingly, a ductal flow reduction expected for a smaller fetus is not established. As a result, the percentage of ductal shunting in IUGR compared to normal fetuses is a lot greater throughout the gestation. This demonstrates the function of DV in maintaining sufficient amount of oxygen to the brain and myocardium, by means of a constant blood flow, despite a placenta disease and consequently a reduced umbilical blood flow. Another result by Bellotti was a significant increase of ductal isthmus diameters in IUGR foetuses.

Interestingly, Kiserud et al. [26] have investigated the degree of shunting though ductus venosus in IUGR fetuses as well. In the article *Ductus venosus shunting in growth-restricted fetuses and the effect of umbilical circulatory compromise* it is stated that the degree of shunting though DV is higher in presence of IUGR, and consequently, the flow to the liver is minor. These findings were particularly related to those with considerable

umbilical hemodynamic compromise. Furthermore, the relatively large cross-sectional area of the DV is especially the reason for a high degree of shunting through that vessel. Another interestingly finding is the shift of the diameter ratio of the ductus venosus and umbilical vein in the direction of a relatively wider ductus venosus allowing increased transmission of pulsations from the ductus venosus towards the umbilical vein. This is a clinical sign of fetal compromise in these fetuses.

All the above diseases are listed in the table below, where the typical sign related to fluid mechanics are pointed out.

3.0.11 Table of the Various Diseases Related to Ductus Venosus

Disease	Geometry	Signs
Chromosomal Abnormalities		significantly lower A,S and D waves. higher PIV. Absent or reversed flow during atrial contraction
Cardiac defects		augmented a-wave
Hypoxemia	increased DV /UV diameter	pulse waves transmitted into the UV increased flow thourgh DV
IUGR	Increased DV/UV diameter	Increased DV shunting, reduced flow in LPV and pulsation in the umbilical vein

In the following, reduced mathematical models will be presented. In this thesis, a 1D model have been utilized whereas 0D models have been applied as boundary conditions. This results in a Multiscale model. A more in depth presentation can be found in the project [1]. The method used in this thesis will be enhanced in section 7. An introduction of reduced models will be explained briefly in section 3.1

3.1 Lumped Models (0D)

Zero dimensional, or lumped parameter models assume a uniform distribution of several variables such as pressure, volume and flow making it more easy to apply. However, in contrast to the higher dimensional models, variation of these parameters in space, within a compartment, cannot be recognized. Zero dimensional models results in a set of simultaneous ordinary differential equations (ODEs). There are often two ODEs for each compartment, both conservation of mass and momentum which are further supplemented with an algebraic equilibrium equation relating volume to pressure, see section 7.2 [35]. Furthermore, these models are developed to deal with global hemodynamics within the whole circulation system. A similarity between blood flow in the circulatory system and electric conduction in a circuit is found, which can further be described as the pressure gradient that forces the blood to flow against the hydraulic impedance (representing frictional loss, vessel wall elasticity and blood inertia) compared to voltage gradient in a circuit which force the flow to be driven against the electric impedance (representing resistance, capacitance and inductance). However, it must be stated that the electrical analogue is unable to describe the non-linearities, meaning the convective acceleration terms in the momentum equation and/or the non-linear relation between pressure and volume that will occur in real blood vessels. 0D cardiovascular system analysis has its origin using the Windkessel model, which models the arterial flow. Lumped parameter models can for example be models of the heart, vessel, circulatory system (connecting heart and vessel compartments) and models for modelling the terminal vessels, such as boundary condition for 1D networks. The latter is applied in this thesis where they represent the resistance of the umbilical vein, ductus venosus and left portal vein.

3.1.1 Windkessel models

The windkessel is a lumped model, meaning that it can only describe the whole arterial system in terms of a pressure-flow relation at its entrance with two parameters that have a physiological meaning. This tends to a drawback with the windkessel model. It is impossible to describe neither the wave travel nor reflections of waves inside the arterial tree. However, the main advantage with the windkessel model is that it only contains few parameters that represent the main properties of the arterial tree [24].

[1] Modelling the human cardiovascular system

3.1.2 Two Element Windkessel

The two Windkessel model describe the hemodynamics of the arterial system in form of compliance and resistance. It can explain the pressure decay in the aorta during diastole, but fell short in systole. The model was originally developed with the aim to estimating cardiac output from pressure measurements in the aorta. The two element Windkessel model yields an input impedance modulus, which represents well the input impedance in the aorta in the frequency domain, but leads to a drawback at high frequencies where it falls asymptotically to zero [24].

3.1.3 Three Element windkessel

An improved model, namely the three element Windkessel was made. A new third term, namely the characteristic impedance Z_c was introduced. This term forms a link between the lumped windkessel model and wave travel appearance of the arterial system. Z_c was connected with the two-element in series, leading to a considerable improvement of the medium-to high frequency range of the model. As a result, the three-element windkessel model can show realistic pressure and flow wave shapes. However, for low frequencies, errors are obtained [24].

3.1.4 R,L and C Coefficients

3.1.5 Resistance

The coefficient $R = \frac{\rho K_R l}{(A_0)^2}$ represents the resistance induced to the flow by the blood viscosity. R can be obtained differently for various velocity profiles or if a non- Newtonian rheology is introduced.

3.1.6 Inertia (Inductance)

The coefficient $L = \frac{\rho l}{A_0}$ represents the inertial term

3.1.7 Compliance (capacitance)

The compliance represent the mass storage term in the mass conservation law, due to the *compliance* of the vessel

A complete presentation of the lumped parameter model utilized in this thesis is demonstrated in section 7.2

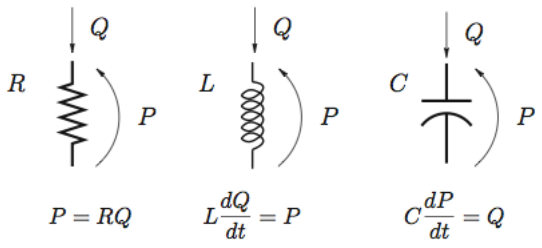

Figure 5: Figure illustrating the R,L and C coefficients. Taken from [13]

3.2 Distributed and 1D Models

Distributed models are created by breaking up the arterial tree into small compartments with known geometry and mechanical properties. The wave transmission characteristics of each arterial compartment can be described using Womersleys oscillatory flow theory or electrical transmission line theory. In addition, distributed models of the arterial tree can be established based upon the 1D form of the Navier Stokes equations for both conservation of mass and momentum [8] . The latter have been utilized in this thesis, and the set up of the mathematical model will be presented in section 7 .

Distributed models are used at high frequencies where the wavelength approaches the physical dimensions of the circuit, making the lumped models inaccurate. When 0D models give a globally lumped description of the arterial tree, and do not account for pressure nor flow wave propagation in the arterial tree, distributed models satisfy both arterial geometry and wall elasticity complications. Many 1D models for the vessel network have been established to study the wave propagation in various applications [9] [34] [5]. The main difference between these models were the boundary conditions applied and also the method used as solution.

The motion of the blood flow is governed by the incompressible continuity and 1D Navier Stokes equations, while the vessel wall, either elastic or viscoelastic, is governed by the equilibrium equations. Accordingly, several complications occurs when dealing with 1D pulse wave propagation. This can either be a discontinuity of the material properties, such as variation of the youngs modules, E ,or a sudden change in cross sectional area due to pathologies, e.g. an aneurysm, considerable change in impedance at the junction between the Ductus Venosus and the umbilical vein [33] occurrence of bifurcation or curvature and nonlinear pressure/area relation for the vessel wall etc. [13]

Based on the 1D mass conservation equation 28 and conservation of momentum29, gives rise to several different wave propagation models by Including different terms and different assumptions [5] [8] [34]. Further in this thesis, the assumptions that have been made will be presented and enhanced.

3.3 Wave Intensity Analysis

"Wave energy" is referred to the fluids total energy, which is associated with a wave. Contrarily, "wave intensity" is referred to the rate of wave energy that is transported. Moreover, the instantaneous power the wave carries per unit cross sectional area. [2] The wave has both kinetic energy that is associated with the velocity of flow, and potential energy which relates to the expansion of the arterial wall, since blood is considered incompressible.
This is a one-dimensional analytical technique to achieve information regarding the wave travel at a certain location in the circulation. In order to perform wave intensity analysis, only flow velocity data and pressure (or arterial diameter changes) retrieved from the same measurement are required. Furthermore, wave intensity analysis may only provide information about the direction of the travelling wave. In what way this can be implemented is briefly described below.

In practice, it means that if the pulse wave and blood travels in the same direction, the velocity will increase, contrary, if the pulse travels in the opposite direction of blood, it will cause a velocity deflection [33]. This is demonstrated in figure 6

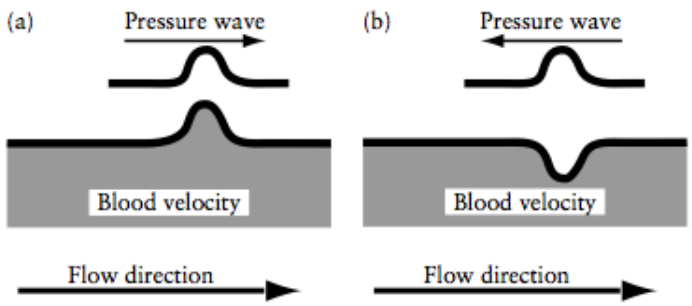

Figure 6: Concept of wave intensity. (a) corresponds to the pulse wave and blood flow travelling in the same direction, and (b) pulse wave and blood flow in opposite direction. Taken from [33]

In this thesis, the different vessels have different boundary conditions. Hence, the three vessels respond differently to the various signals applied. Most interestingly is the signal at DV, creating a pulsatile flow due to a pressure varying in time. The pressure signal at DV and the network respond are illustrated in figure 7, 8, 9 and 10. The figures are in good agreement with the above *wave intensitity analysis*. It must be stated that the vessels have different positive directions defined in terms of the pressure applied at DV. And as already mentioned, the flow waves will therefore interfere differently. In this thesis, the applied flow takes place at the inlet of UV, and the flow distribution is illustrated in figure
reffig:flowdist The flow waves in LPV travels in the same direction of the pressure waves, while the flow waves in UV and DV travels in the opposite direction of the pressure waves,

creating a negative flow wave deflection.

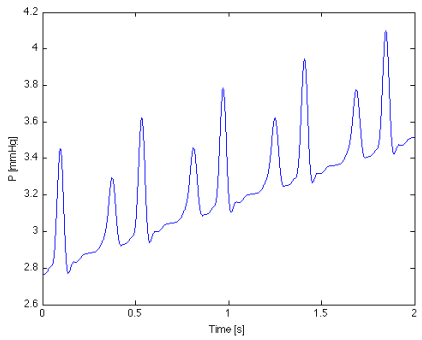

Figure 7: The signal applied at ductus venosus

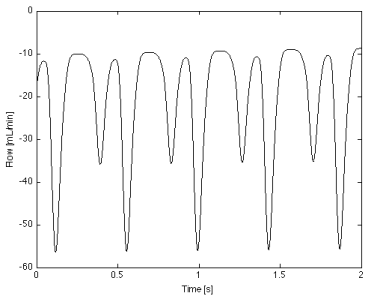

Figure 8: DV

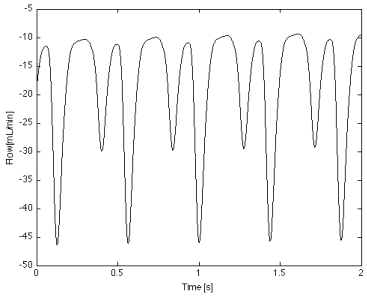

Figure 9: UV

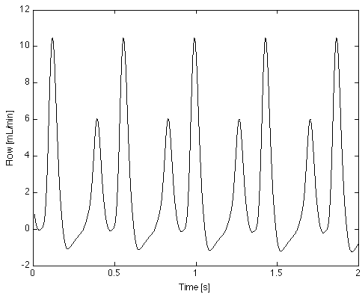

Figure 10: LPV

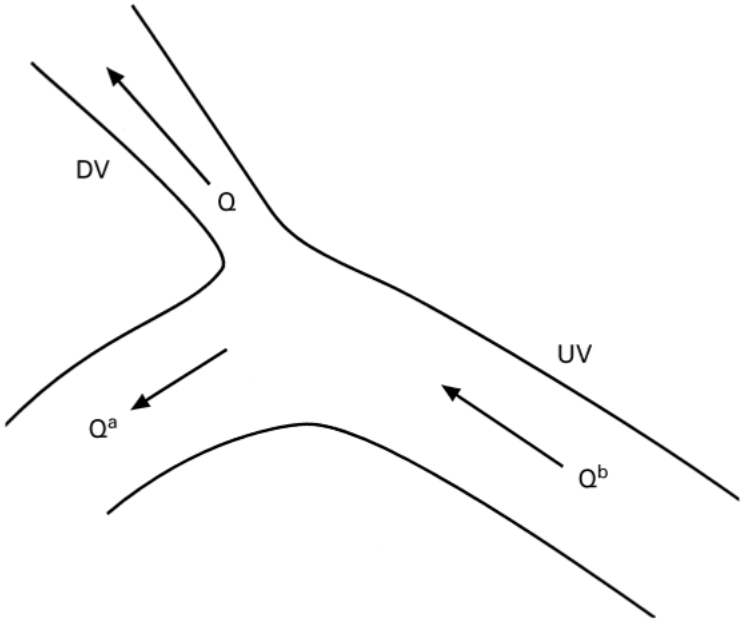

Figure 11: Flow distribution of the umbilical vein (UV), ductus venosus (DV) and left portal vein. Q^b denotes the flow in the umbilical vein before the bifurcation, while Q^a represents the flow transmitted into the left portal vein. Q is the flow transmitted through DV

3.3.1 Wave Separation

Several methods have been suggested to separate measured pressure and flow into forward and backward travelling components [14]. The waves travelling towards the periphery from the heart consists of information about the hearts condition. The reflected waves consists of information regarding the periphery. This method has been highly significant when it comes to analysing the human cardiovascular system. In this thesis, the method will be applied to the human fetus, i.e, umbilical vein, left portal vein and ductus venosus, where the pressure waves coming from the heart contain information about the fetal heart, and the flow waves from the umbilical vein contain information regarding the placenta.

The method utilized in this thesis, was suggested by Westerhof et al [14], and is based on the linearised and inviscid form of the governing equations, elaborated in section 7.1.

$$C\frac{\partial p}{\partial t} + \frac{\partial Q}{\partial x} = 0 \tag{3}$$

$$\frac{\partial Q}{\partial t} + \frac{A}{\rho}\frac{\partial p}{\partial x} = 0 \tag{4}$$

After cross derivation and subtraction of the above equations, the classic wave equations are obtained:

$$\frac{\partial^2 Q}{\partial t^2} + c^2\frac{\partial^2 Q}{\partial x^2} = 0 \tag{5}$$

$$\frac{\partial^2 p}{\partial t^2} + c^2 \frac{\partial^2 p}{\partial x^2} = 0 \tag{6}$$

where

$$c^2 = \frac{A}{\rho C} \tag{7}$$

moreover, c is defined as:

$$c = \sqrt{\frac{A}{\rho C}} \tag{8}$$

equation 8 is also known as the Bramwell - Hill equation [1].

The wave equations have the general solution

$$P = P_0 f(x - ct) + P_0^* g(x + ct) \tag{9}$$

$$Q = Q_0 f(x - ct) + Q_0^* g(x + ct) \tag{10}$$

where f and g represent the forward and backward propagating waves with wave speed c.

Inserting the wave equations obtained in equation 9 and 10 into the linearized momentum equation 4 yields

$$-cQ_0 f' + cQ^* g' + \frac{A}{\rho} P_0 f' + \frac{A}{\rho} P^* g' = 0 \tag{11}$$

$$f'(\frac{A}{\rho} P_0 - cQ_0) + g'(\frac{A}{\rho} P^* + cQ^*) = 0 \tag{12}$$

Both equations must hold for arbitrary f and g and the characteristic impedance Z_c becomes

$$Z_c = \frac{c\rho}{A} \tag{13}$$

The characteristic impedance may also be expressed by means of the pressure and flow such as

$$Z_c = \frac{P}{Q} = \frac{P_f}{Q_f} = -\frac{P_b}{Q_b} \tag{14}$$

From the expressions above, the characteristic impedance is seen as the ratio of the pulsatile flow and pressure components in case of a unidirectional wave, i.e. in absence of reflections. Moreover, Z_c may also express the ratio of local inertance (ρ/A) to compliance C, and becomes

$$Z_c = \sqrt{\frac{\rho}{A} \frac{1}{C}} \tag{15}$$

where $c = \sqrt{\frac{A}{\rho} \frac{1}{C}}$ and $C = \frac{\partial A}{\partial p}$.

3.3.2 Wave Reflections

Wave reflections may easily be understood as a single travelling pulse towards an end where it is reflected. However, for a train of pulses or continuous oscillations, the reflected waves will interfere with the original pulse, and the only evidence of reflections is the spatial variations in the waves amplitude. Reflections occur when a change in the characteristic impedance is present. Furthermore, the reflection factor Γ can be obtained by

$$\Gamma \equiv \frac{p_b}{p_f} = -\frac{Q_b}{Q_f} \tag{16}$$

where

$$p = p_f + p_b, Q = Q_f + Q_b \tag{17}$$

Then, the forward and backward travelling pressure and flow can be expressed by the characteristic impedance:

$$P = P_f + P_b, Q = Q_f + Q_b = \frac{p_f}{Z_c} - \frac{p_b}{Z_c} \tag{18}$$

after som algebraic elimination, the forward and backwards propagating pressure waves becomes

$$p_f = \frac{p + Z_c Q}{2}, p_b = \frac{p - Z_c Q}{2} \tag{19}$$

And the forward and backward propagating flow waves becomes

$$Q_f = \frac{Q + P/Z_c}{2}, Q_b = \frac{Q - P/Z_c}{2} \tag{20}$$

The propagation of pressure and flow waves in the arterial system may establish information about stenotic regions, aneurysms and other vascular diseases [14].

4 Physical and Mathematical Background

Deriving the governing equations, assumptions regarding area-mass flux (A, Q), area-velocity (A, u), pressure-velocity (p, u) and pressure-mass flux (p, Q) variables are discussed. The non-linear hyperbolic system expressed in (A, u), the extension of a single vessel model into a more complete network of vessels can be done by characteristics decomposition combined with conservation of mass and total pressure. When it comes to more widely linearised system, conservation of static pressure has to be applied. For the linearised system can additionally include the derivation of a reflected coefficient. The derivation of the fundamental equations in conservative and characteristic variables gives basic information for several numerical approaches [27].

In sections 4.1 and 4.2 the conservation of mass and momentum starting from a control volume state will be derived. It will be shown that applying the mass conservation statement to a control volume gives rise to the derivation of the Windkessel equation which is used in reduced modelling of the arterial system. see section 4.2.1 It must be stated that as it regards the Windkessel model, it does not yield information about the dynamics of the system along the vessel, where the 1D dimensional models advances.

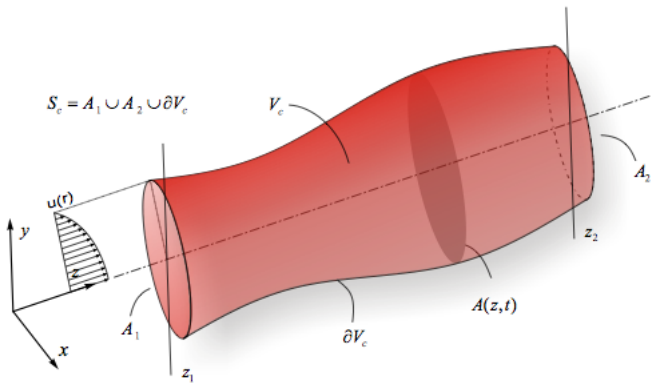

Figure 12: A compliant vessel with axial coordinate z and surface area A(z,t). Illistration taken from [14]

4.1 Mass Conservation

Defining the control volume as shown in figure 12, the rate of change of mass plus the net mass flux out of the control volume has according to the mass conservation be equal to zero. Defining $V(t) = \int_0^l A dx$ where l is the length of the vessel, the conservation can be written as

$$\rho \frac{dV(t)}{dt} + \rho Q(l,t) - \rho Q(0,t) = 0 \tag{21}$$

By inserting the definition of V into 21, and further assuming l independent of time, the equation becomes

$$\rho \int_0^l \{\frac{\partial A}{\partial t} + \frac{\partial Q}{\partial x}\} dx = 0 \tag{22}$$

This equation has to be valid for any value of l due to the non specified length, in general it is required that the integrand is zero. Therefore, the one-dimensional mass conservation equation becomes

$$\frac{\partial A}{\partial t} + \frac{\partial Q}{\partial x} = \frac{\partial A}{\partial t} + \frac{\partial uA}{\partial x} = 0 \tag{23}$$

A statement to this is, by introducing the vessel compliance C, defined as $C = \frac{dV}{dP}$ where P is an appropriate average of the pressure p over length l, and further applying the chain rule in combination with equation 21 tends to

$$\frac{dP}{dt} = \frac{dP}{dV}\frac{dV}{dt} = \frac{Q(0,t) - Q(l,t)}{C} \tag{24}$$

4.2 The 1D momentum balance

By considering the vessel as our control volume and further assume no flux though the side walls in the x-direction, the momentum equation states that the rate of change of momentum within the control volume plus the net flux of momentum out of the control volume can be seen as the equation to the applied forces on the control volume and can be expressed over an arbitrary length l as

$$\frac{d}{dt}\int_0^l \rho Q dx + (\alpha\rho Q u)_l - (\alpha\rho Q u)_0 = F \tag{25}$$

Then a statement that $Q = Au$ is made and define F as the applied forces in the x-direction acting on the control volume. Since $\rho Q = \rho u A = \rho \int_S \hat{u} d\sigma$ represents the x-momentum integrated over the section S, the left hand side of equation 25 is similar to the left hand side of the mass conservation given by equation 4.1. However, an introduction to the momentum flux correction α accounting for the non-linearity of the sectional integration in therms of the local velocity $\hat{u}$ i.e.

$$\int_S \rho(\hat{u})^2 d\sigma = \alpha\rho u^2 A = \alpha\rho Q u -> \alpha(x,t) = \frac{\int_S \hat{u}^2 d\sigma}{Au^2} \tag{26}$$

For a uniform flow profile over a section $\alpha = 1$

Further, by defining the applied force F, involving a pressure and viscous force contribution, treating the tube as axisymmetric, assuming l independent of time and ρ constant, the one-dimensional momentum equation becomes

$$\frac{\partial Q}{\partial t} + \frac{\partial(\alpha Q u)}{\partial x} = -\frac{A}{\rho}\frac{\partial p}{\partial x} + \frac{f}{\rho} \tag{27}$$

where a simplification to the right-hand side pressure gradient term has been made.

The governing one-dimensional system in terms of the variables (A, Q) can be expressed as

$$\frac{\partial A}{\partial t} + \frac{\partial Q}{\partial x} = 0 \tag{28}$$

$$\frac{\partial Q}{\partial t} + \frac{\partial \alpha Q^2/A}{\partial x} = -\frac{A}{\rho}\frac{\partial p}{\partial x} + \frac{f}{\rho} \tag{29}$$

For deeper explanation see [14]

4.2.1 Solutions to the the Windkessel

The whole arterial system modelled as one single compliant chamber.

As described in section **??** Mass conservations can be defined as:

$$\frac{dV}{dt} = \frac{dV}{dP}\frac{dP}{dt} = C\frac{dP}{dt} = Q - Q_p = Q - \frac{P}{R}$$

Windkessel model :

$$\frac{dP}{dt} + \frac{1}{RC}P = \frac{Q(t)}{C} \tag{30}$$

With the homogenios solution

$$P_h = \hat{P} \exp - \frac{(t - t_0)}{\tau} \tag{31}$$

where

$$\tau = RC = R\frac{dV}{dP}$$

$$P(t) = P \exp - \frac{(t - t_0)}{\tau} + \frac{1}{C} \int_t o^t Q(t') \exp \frac{(t' - t)}{\tau} dt' \tag{32}$$

4.2.2 Impedance of 2WK

$$\frac{dP}{dt} \frac{1}{RC} P = \frac{Q}{C}$$

proposed solutions : $P = \hat{P} \exp(i\omega t), Q = \hat{Q} \exp(j\omega t)$

$$\frac{dP}{dt} = j\omega \hat{P} \exp j\omega t$$

The input impedance becomes:

$$Z = \frac{R}{\sqrt{1 + (\omega RC)^2}} \tag{33}$$

with the phase angle:

$$< Z = - \arctan \omega RC \tag{34}$$

4.2.3 Three Element Windkessel

$$P - P_d = Z_Q \tag{35}$$

From (2WK)

$$C\frac{dP_d}{dt} + \frac{P_d}{R} = Q \tag{36}$$

to eliminate P_d by substitution of 35 into 36 :

$$C\frac{dP}{dt} + \frac{P}{R} = Q(1 + \frac{Z_c}{R}) + Z_c C\frac{dQ}{dt} \tag{37}$$

By introducing the harmonic solution, the input impedance now becomes:

$$Z = Z_c + \frac{R}{1 + j\omega RC} = \frac{R + Z_c + j\omega Z_c RC}{1 + j\omega RC} \tag{38}$$

Taken from [14]

5 The Uncertainty of Biological Systems

Modelling the pressure and flow wave propagation in the human arterial system has received considerable attention. However, minor has been made concerning the uncertainty in data. The biological systems are uncertain by nature due its non-linearities. This makes the reduced and simplified models demanding in order to recapture the systems correctly. Furthermore, the impact of errors, or uncertainty, such as parameter values, initial and boundary conditions have been lacking consideration. The aim of uncertainty analysis is to investigate the errors providing more reliable results. Therefore, rather than dealing with numerical errors afterwards, the uncertainty should be included at the beginning. Especially for non-linear problems, uncertainty in data may provide great differences in the output that can not be neglected [4]. Moreover, reliable assessment of the system behaviour can not be made without knowledge of the impact regarding the uncertainty that is present [28]. For the human fetus circulation, numerous parameters contain an uncertainty. The explanation to this is either due to the non existing data caused by complicated or even impossible measurements, the high variation within the individual fetuses or dissimilarities caused by a pathological condition.

6 Stochastic Framework

In order to assess the influence on the result, the model parameters in the arterial network system need stochastic contributions. Defining uncertain model parameters as continuous random variables, the deterministic partial differential equations (PDE) are converted to stochastic PDEs. There exists several approaches to solve this system. In this thesis, the system is solved by a deterministic solver combined with generalized poychaos method. *Vascular polychaos* has been applied combined[2], where *Vascular polychaos* combines *Vascular 1Dflow*[3] with Polynomial toolbox[4]. Polychaos approximate the solution with general polynomial chaos expansion(gPCE).

[2]Master thesis by Vinzenz Eck
[3]Leinan P.R, Hellevik L.R
[4]Jonathan Feinberg

6.1 Sensitivity Analysis

The sensitivity of a simulation is defined as the relative change in time and amplitude of flow and pressure waves that occur at a certain place in the network. The relative change is due to the uncertain parameters. There exists numerous parameters that are uncertain within an arterial network system, whereas in this study, only a few will be taken into account. In addition, only flow waves will be explored. Furthermore, the mean (expected) value, standard deviation (STD) and 99% confidence intervals are used as sensitivity measurements. The gPCE calculate these sensitivity measures with methods from the polynomial chaos toolbox.

The sensitivity of flow waves will be calculated for the total flow signal, where all the uncertain parameters are taken into account, explored in figures demonstrating the mean value and STD. As a result, the mean values and the STD provide an overall variability of the uncertain solution.

In addition, the sensitivity due to a specific uncertain parameter will be presented by the mean value, STD and confidence interval. Accordingly, the sensitivity of peaks can be analysed. The change in time and amplitude are supplemented with figures demonstrating the confidence interval and STD of the specific peaks that is chosen. The confidence intervals are calculated for the time and amplitude of the chosen peaks and forecast the extent with a 99 % confidence. Moreover, the confidence interval lines presents the same information as the STD box plots, however, they also show the impact on the simulation by visualising the prediction of the peaks appearance with a 99% confidence.

As already mentioned, the peaks during systole, diastole and atrial contraction are of significant relevance when examining the fetal well being. The STD for each peak will be illustrated by means of box plots whereas the yellow represent the total STD, and the blue box represent the partial STD. This gives rise to a comparison between the sensitivity of the various vessels with respect to the total and partial STD. Both confidence interval and STD box are illustrated in figure 13

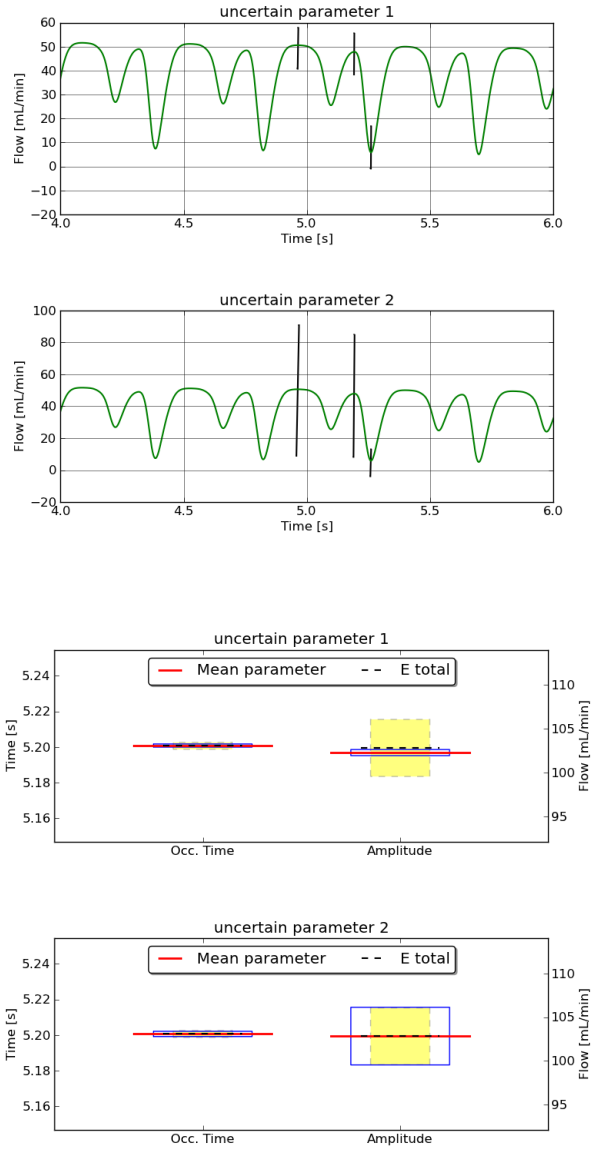

Figure 13: Top: an example of a confidence interval with two uncertain parameters. bottom: an example of STD with two uncertain parameters

7 Methods

7.1 Governing Equations

The governing equations for flow in a compliant vessel having a circular cross section, see figure 14, are derived from integration of the axial continuity and Navier-Stokes momentum equation.

$$\frac{\partial A}{\partial t} + \frac{\partial Q}{\partial z} = 0 \tag{39a}$$

$$\frac{\partial Q}{\partial t} + \frac{\partial}{\partial z}\left(2\pi \int_0^R r v^2 dr\right) + \frac{A}{\rho}\frac{\partial P}{\partial z} = -2\pi\frac{\mu}{\rho}\left[\frac{\partial v}{\partial r}\right]_{r=R} \tag{39b}$$

The blood is assumed to behave as a Newtonian fluid having a density ρ equal to 1060 Kg m^{-3} and a viscosity μequal to 0.004 Pa s. The second and fourth term in equation 39b are the convective acceleration and the friction force on the viscous wall respectively and they depend on the velocity profile in a local cross section. The set of equations have three primary variables A, P and Q that are average quantities over the cross sections of the vessels depending on the position along the vessel and time and are defined as:

$$A(z,t) = 2\pi \int_0^{R_{(z,t)}} r dr \tag{40a}$$

$$Q(z,t) = 2\pi \int_0^{R_{(z,t)}} r v(z,r,t) dr = A(z,t) v_z(z,t) \tag{40b}$$

$$P(z,t) = \frac{2\pi}{A(z,t)} \int_0^{R_{(z,t)}} r p(z,r,t) dr \tag{40c}$$

Where $A = A(z,t)$ is the lumen area, $Q = Q(z,t)$ is the volumetric flow rate, $P = P(z,t)$ is the mean pressure and $v_z = v_z(z,t)$ is the mean axial velocity

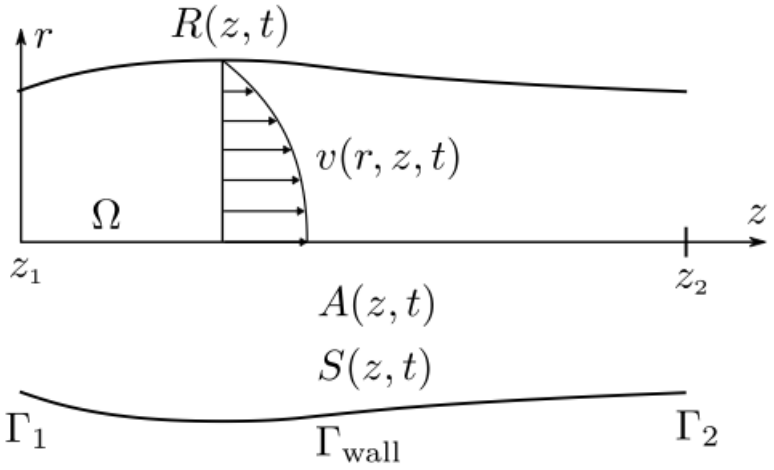

Figure 14: A wessel wall segment illustrating its compliant structure with a circular cross-section, where the lumen radius R=R(z,t); the lumen area A=A(z,t); the antisymmetric velocity profile v(z,r,t); the left flow boundary surface Γ_1 at z_1, and Γ_2 at the flow boundary surface z_2

7.2 Generalized Polynomal Chaos

Some General Expressions

Expected Value

The expected, or mean value of a continuous random variable is the average of all real numbers, defined as

$$\mu = E(z) = \int_{-\infty}^{\infty} zp(z)dz \tag{41}$$

where $P(z)$ is the probability density function, describing the probability distribution of the continuous random variable z.

Variance

The variance is the measurement of the variation of a continuous random variable, defined as

$$\sigma^2 = Var(z) = \int_{-\infty^{\infty}} (z-\mu)^2 p(z)dz \tag{42}$$

Standard Deviation

The standard deviation is the spreading of a stochastic variable, defined as

$$\sigma = STD(z) = \sqrt{Var} = \sqrt{\sigma^2} \tag{43}$$

Furthermore, the solution of $u(x,t,z)$ can be achieved by applying the generalized polynomial chaos expansion (gPCE), determining the uncertainty. In gPCE, the system solution is expanded as finite-term orthogonal polynomials series of the input variables

$$u(x,t,z) \approx \hat{u}(x,t,z) = \Sigma c_i(x,t)\phi_i(z) \tag{44}$$

where $c_i(x,t)$ is Fourier coefficient and $\phi_i(z)$ is the continuous random variables [28].

Constitutive Model

The governing equation contains of two differential equations with three primary variables (A, P and Q). In order to complete the set of equations, a constitutive relation is in need. Hence, the compliance C is introduced as a connection of the area A and pressure P.

The compliance is expressed as

$$\frac{\partial A}{\partial P} = C(z,t,P). \tag{45}$$

In general, the compliance is a factor depending on the location in the vascular three and time through viscoelastic effects. However, in this thesis it is assumed to be pressure dependant, thus $C = C(P)$

The constitutive model becomes

$$A(p) = A_0 + C(P - P_0) \tag{46a}$$

and by using the chain rule the equation 47 is obtained.

$$\frac{\partial A}{\partial t} = \frac{\partial A}{\partial P}\frac{\partial P}{\partial t} = C\frac{\partial P}{\partial t} \tag{47}$$

The system is closed by including the vascular compliance and substituted into the equations of continuity and momentum.

$$\frac{\partial P}{\partial t} + \frac{1}{C}\frac{\partial Q}{\partial z} = 0 \tag{48a}$$

$$\frac{\partial Q}{\partial t} + \frac{\partial}{\partial z}\frac{Q^2}{A}\frac{A}{\rho}\frac{\partial p}{\partial z} = 0 \tag{48b}$$

$$\frac{\partial A}{\partial t} + \frac{\partial Q}{\partial z} = 0 \tag{48c}$$

Cross-derivation and subtraction of the above equations 48 (a) and (b) leads to

$$\frac{\partial^2 p}{\partial t^2} - c_0^2\frac{\partial^2 p}{\partial z^2} = 0 \tag{49a}$$

$$\frac{\partial^2 Q}{\partial t^2} - c_0^2\frac{\partial^2 Q}{\partial z^2} = 0 \tag{49b}$$

where the *pulse wave velocity* for inviscid flows have been introduced:

$$c_0^2 = \frac{dP}{dA}\frac{A}{\rho} = \frac{1}{C}\frac{A}{\rho} \tag{50}$$

System Equations

In this thesis the governing for flow in a compliant vessel has been chosen by a three equation system, representing the three primary variables A, Q and P. The system can be closed by introducing the vessel compliance by substituting into the continuity equation. Furthermore, the velocity profile is given by

$$v(z, r, t) = \phi(r)v_z(z, t), \tag{51}$$

where $v_z(x, t)$ is the mean (cross sectional) axial velocity. The velocity profile that is chosen is the power law given by

$$\phi(r) = \frac{\gamma + 2}{\gamma}\left(1 - \left(\frac{r}{R}\right)^{\gamma}\right), \tag{52}$$

where R is the radius of the vessel, and where γ determines the bluntness of the velocity profile. The non-slip condition at the vessel wall is satisfied with $\phi(R) = 0$. Furthermore, $\gamma = 2$ gives Poiseuille flow [**?**].

By substituting equation 51 and 52 into the momentum balance gives

$$\frac{\partial A}{\partial t} + \frac{\partial Q}{\partial z} = 0, \tag{53}$$

$$\frac{\partial Q}{\partial t} + \delta\frac{\partial}{\partial z}\left(\frac{Q^2}{A}\right) + \frac{A}{\rho}\frac{\partial P}{\partial z} = -2\pi(\gamma + 2)\frac{\mu}{\rho}\frac{Q}{A}, \tag{54}$$

$$\frac{\partial P}{\partial t} + \frac{1}{C}\frac{\partial Q}{\partial z} = 0 \tag{55}$$

where $\frac{(\gamma+2)}{(\gamma+1)} = \delta$. A normal approach to model 1D vascular flow is to take advantage of a two equation system. Moreover, the most general is the system including equation 53 and 54 with A and Q as primary variables. Another possibility is the set of equation 54 and 55 with P and Q as primary variables, where the pressure-area relation is provided by the compliance C ($\frac{\partial A}{\partial P}$). However, in this study the three equation system including equation 53, 54 and 55 is utilized.

The above system can be presented in matrix notation as:

$$\frac{\partial \mathbf{u}}{\partial t} + \mathbf{M}(\mathbf{u})\frac{\partial \mathbf{u}}{\partial z} = \mathbf{b}(\mathbf{u}), \mathbf{u} = \begin{bmatrix} P \\ Q \\ A \end{bmatrix} \tag{56}$$

where

$$\mathbf{M} = \begin{bmatrix} 0 & \frac{1}{C} \\ Cc^2 - \delta v_z^2 C & 2\delta v_z \end{bmatrix}, \mathbf{b} = \begin{bmatrix} 0 \\ -2\pi(\gamma+2)\frac{\mu}{\rho} v_z \end{bmatrix} \tag{57}$$

and where $Cc^2 = A/\rho$ and $v_z = Q/A$.

Numerical Discretization and Scheme

The vessels are discretized with grid nodes $i = 1, .., N$ and vessel length $L = \delta x(N-1)$, where N is the number of grid points and δx is the distance between the grid nodes and Δt is the time step. A forward-backward MacCormack scheme have been applied in order to solve the system

for $i = 2, .., N-1$

$$\overline{\mathbf{u}}_i^{n+1} = \mathbf{u}_i^n - \Delta t \left[\mathbf{H}(\mathbf{u}_i^n) \frac{\mathbf{u}_{i+1}^n - \mathbf{u}_i^n)}{\Delta x} + \mathbf{b}(\mathbf{u}_i^n) \right] \tag{58}$$

$$\mathbf{u}_i^{n+1} = \frac{1}{2}(\mathbf{u}_i^n + \overline{\mathbf{u}}_i^{n+1} - \Delta t \left[\mathbf{H}(\overline{\mathbf{u}}_i^{n+1} \frac{\overline{\mathbf{u}}_i^{n+1} - \overline{\mathbf{u}}_{i-1}^{n+1}}{\Delta x} + \mathbf{b}(\overline{\mathbf{u}}_i^{n+1}) \right] \tag{59}$$

Eguation 58 is the predictor step and equation 59 is the corrector step. However, the boundary nodes $i = 1, N$ require to be solved, and will therefore be established in a characteristic manner.

Characteristic Analysis

The eigenvalues of the system matrix $\mathbf{M}$ are given by:

$$\lambda_{1,2} = \delta \mathcal{M} \rfloor \pm c' \tag{60a}$$

$$c' = c\sqrt{1 + \delta(\delta - 1)\mathcal{M}^2} \tag{60b}$$

where c is the pulse wave velocity and $\mathcal{M} = v_z/c$ is the Mach number. Furthermore, the left and right eigen-matrices and the diagonal eigenvalue matrix are defined as:

$$\mathbf{L} = \begin{bmatrix} \mathbf{1}_1^T \\ \mathbf{1}_2^T \end{bmatrix} \mathbf{R} = \begin{bmatrix} \mathbf{r}_1 & \mathbf{r}_2 \end{bmatrix} \Lambda = \begin{bmatrix} \lambda_1 & 0 \\ 0 & \lambda_2 \end{bmatrix} \tag{61}$$

where $\mathbf{1}_j^T$ and $\mathbf{r}_j$ for $j = 1, 2, 3$ are the left and right eigenvector respectively of the system matrix $\mathbf{M}$. Moreover, $\mathbf{R}(\mathbf{u})$becomes

$$\mathbf{R} = \begin{bmatrix} Z_1 & Z_2 \\ 1 & -1 \end{bmatrix} \tag{62}$$

$$\mathbf{L} = \frac{1}{Z_1 + Z_2} \begin{bmatrix} 1 & Z_2 \\ 1 & -Z_1 \end{bmatrix} \tag{63}$$

Where $Z_1 = \frac{1}{\lambda_1 C}$ and $Z_2 = \frac{-1}{\lambda_2 C}$

The differential system given in equation 56 can now be given in the equivalent form by substitution of equation 61

$$\mathbf{L}\frac{\partial \mathbf{u}}{\partial t} + \mathbf{\Lambda}\mathbf{L}\frac{\partial \mathbf{u}}{\partial z} = \mathbf{L}\mathbf{b}, \tag{64}$$

A change in variables are introduced by:

$$\frac{\partial \mathbf{w}}{\partial \mathbf{u}} = \mathbf{L}, \tag{65}$$

where $\mathbf{w} = [w_1, w_2, w_3]^T$ is a vector of the characteristic variables. Introduction of the characteristic variables now transforms the system into the following:

$$\frac{\partial \mathbf{w}}{\partial t} + \mathbf{\Lambda}\frac{\partial \mathbf{w}}{\partial z} = \mathbf{L}\mathbf{b}. \tag{66}$$

Therefore, the system in equation 56 contain two non-zero Riemann invariants with two characteristic directions

$$\mathbf{w} = \begin{bmatrix} w_1 \\ w_2 \\ 0 \end{bmatrix} \tag{67}$$

Integration of the Riemann invariants, given in equation 65, combined with the mean value theorem gives

$$\Delta \mathbf{w} = \int_{\mathbf{u}^n}^{\mathbf{u}^{n+1}} \frac{\partial \mathbf{w}}{\partial \mathbf{u}} d\mathbf{u} = \int_{\mathbf{u}^n}^{\mathbf{u}^{n+1}} \mathbf{L}(\mathbf{u}) d\mathbf{u} = \mathbf{L}(\hat{\mathbf{u}})\Delta \mathbf{u} \tag{68}$$

where $\mathbf{u}^n \leq \hat{\mathbf{u}} \leq \mathbf{u}^{n+1}$.

Boundary Conditions

The boundary nodes $i = 1, N$ at the surfaces Γ_1 and Γ_2 is updated by the boundary variable $\mathbf{u}^{n+1} = \mathbf{u}^{n+1}_{i=1,N}$

$$\mathbf{n}^{n+1} = \mathbf{u}^n + \mathbf{R}(\hat{\mathbf{u}})\Delta \mathbf{w} \tag{69}$$

in the interval $\Delta t = t^{n+1} - t^n$.

further on, the predictor and corrector step in the MacCormack scheme, given in equation 58 and 59, the boundary variables update is given by

$$\hat{\mathbf{u}}^{n+1} = \mathbf{u}^n + \mathbf{R}(\mathbf{u}^n)\Delta \mathbf{w} \tag{70}$$

$$\mathbf{u}^{n+1} = \hat{\mathbf{u}}^{n+1} + \mathbf{R}(\hat{\mathbf{u}}^{n+1})\Delta \hat{\mathbf{w}} \tag{71}$$

The main variable update at the boundary nodes are achieved by the Riemann invariants $\Delta\mathbf{w}$. At each boundary, there exists two Riemann invariants, where one of them enter the flow domain and the other one leaving the flow domain. Therefore, at the boundaries Γ_1 and Γ_2 the Riemann invariants that enters the domain $\Delta w_1 = \Delta w_1(\mathbf{u}_0)$ and the one that leaves $\Delta w_2 = \Delta w_2(\mathbf{u}_0)$ have to be prescribed and is given by

$$\Delta\mathbf{w} = \begin{bmatrix} \Delta w_1(\mathbf{u}_0) \\ \Delta w_2 \\ 0 \end{bmatrix} \tag{72}$$

on Γ_1

$$\Delta\mathbf{w} = \begin{bmatrix} \Delta w_1 \\ \Delta w_2(\mathbf{u}_0) \\ 0 \end{bmatrix} \tag{73}$$

on Γ_2

The Riemann invariants that enters the domain can be dependant on a function $\mathbf{u}_0$ depending on the boundary condition model that is chosen. Moreover, the Riemann invariants that leaves the domain can be measured at the boundary at time $t = t^{n+1}$.

Terminal Lumped Models

Terminal lumped models are attached at the end of each vessel, where the impedance can be modelled. Several lumped models are included in this thesis. As elaborated in section 3.1, various models describe different problems. The three element Windkessel, terminal resistance and $\mathcal{L}$ - network are applied and illustrated in figure 15

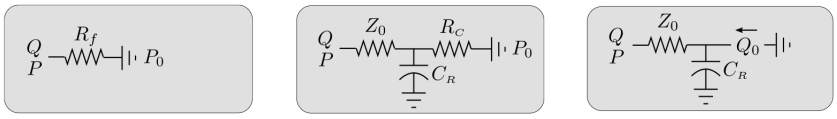

(a) Terminal resistance (b) WK3 (c) $\mathcal{L}$ network

Figure 15: Terminal lumped models, taken from [15]

Three Element Windkessel Model (3WK)

In this thesis, the three element windkessel have been applied. The incremental form of the 3WK is given by

$$\frac{d(\Delta P)}{dt} - \frac{d(\Delta P_0)}{dt} + \frac{\Delta P - \Delta P_0}{R_C C_R} = Z_0 \frac{d(\Delta Q}{dt} + \Delta Q \left(\frac{1}{C_R} + \frac{Z_0}{R_C C_R} \right), \tag{74}$$

where R_C is the Windkessel resistance, C_R is the Windkessel compliance and Z_0 the characteristic impedance.

$$\frac{d\Delta P}{dt} = \frac{d(\Delta w_1 + \Delta w_2)}{dt} \tag{75}$$

Equation 75 demonstrates the pressure derivative after inserting the Riemann invariants given by

$$\Delta P = \Delta w_1 + \Delta w_2 \tag{76}$$

Furthermore, by discretization of the pressure derivatives by a first order scheme gives

$$\frac{d(\Delta P)}{dt} = \frac{(\Delta w_1 - \Delta w_1^n + \Delta w_2 - \Delta w_2^n)}{\Delta t} \tag{77}$$

where Δw_1^n and Δw_2^n are Riemann invariants from the previous time step t=t^n. Having a 3WK connected at the right boundary Γ_2, solving for the Riemann invariant that enters the domain Δw_2 by inserting equation 77 into the 3WK model, having

$$\Delta Q = r_{21}\Delta w_1 + r_{22}\Delta w_2 \tag{78}$$

Δw_2 can be found by

$$\Delta w_2 = \frac{[1 + \tau - r_{21}R_C - r_{21}(1+\tau)]\Delta w_1}{r_{22}R_C} + \frac{\tau(r_{21}-1)\Delta w_1^n}{r_{22}R_C} + \frac{\tau\Delta P_0^n - (1+\tau)\Delta P_0}{r_{22}R_C} \tag{79}$$

where $\tau = (R_C C_R)/\Delta t$, and the characteristic impedance $Z_0 = 1/r_{22}$. Now the boundary variable update can be obtained: $v\mathbf{u}^{n+1} = \mathbf{u}_{i=N}^{n+1}$ for $\Delta\mathbf{w} = [\Delta w_1, \Delta w_2, 0]^T$

$\mathcal{L}$ network compartment

The incremental form of the $\mathcal{L}$ - network compartment is given by

$$\frac{d(\Delta P)}{dt} = Z_0\frac{d(\Delta Q)}{dt} + \frac{(\Delta Q - \Delta Q_0)}{C_R} \tag{80}$$

The compartment is considered at the left of the boundary Γ_1. By solving the Riemann invariant at the entering of the domain w_1, and by following the same procedure as for the 3WK, the $\mathcal{L}$ - network compartment provides

$$\Delta w_1 = -\frac{[1 + \tau_0(r_{22}+1)]\Delta w_2}{(2\tau_0+1)} + \frac{\tau_0(1+r_{22})\Delta w_2^n}{(2\tau_0+1)} + \frac{2\tau_0\Delta w_1^n}{(2\tau_0+1)} + \frac{\Delta Q_0/r_{21}}{(2\tau_0+1)}$$

where $\tau_0 = (Z_0 C_R)/\Delta t$, and the characteristic impedance $Z_0 = 1/r_{21}$. Now by extrapolating Δw_2 from the domain the boundary variable update now becomes $\mathbf{u}^{n+1} = \mathbf{u}_{i=1}^{n+1}$ for $\Delta w = [\Delta w_1, \Delta w_2, 0]^T$

Numerical Model

A 1D model of the DV, IUV and LPV bifurcation has been presented in this thesis. In addition, 0D models representing boundary conditions have been applied in the model. Material and fluid properties have been taken from the literature [15], [18].

The examination of DV, LPV and UV bifurcation are driven by a pressure gradient and volumetric flow, where DV and LPV are simulated with pressures, P_{IVC} andP_{He} and UV with flow Q_{UV} deeper explained in section 7.2. In a study by Haugen et al. venous blood supply to the liver at 36 weeks gestation were investigated [18]. Nevertheless, both the right and left lobe were examined, however, this thesis concerns only the left lobe, hence, some assumptions are made. Haugen et al. discovered a flow coming from the umbilical vein estimated to be 205 mL/min, yet it is set equal to 96.7 mL/min in this study. The reason to this is the loss of blood flow into minor veins along the Inferior Vena Cava (IVC) which are not taken into consideration [15]. Thus, $Q_{0,UV} = 96.7ml/min$. Furthemore, the pressure reservoir at the LPV junction is set equal to $P_{0,He} = 4.3mmHg$.

The pressure at the DV terminal representing the IVC at the inlet to the right atrium is taken from [10]. The pulsatile pressure in the lumped IVC compartment is given by

$$P_{tot,IVC}(t) = P_{0,IVC} + P_{A,IVC}P_{W,IVC}(t) \tag{81}$$

where $P_{A,IVC}$ represents the maximum pressure amplitude, $P_{W,IVC}(t)$ the normalized pressure waveform, and a steady IVC pressure $P_{0,IVC}$

Flow Parameters

The volumetric flow rate Q(t) can be calculated by means of the mean velocity V_mean and cross sectional area A at time t as:

$$Q(t) = V_{mean}(t)A(t) \tag{82}$$

where $V_{mean}(t)$ is defined as:

$$V_{mean}(t) = \frac{1}{A(t)} \int_{A(t)} [\mathbf{V}(t) \cdot \mathbf{n}(t)]dA, \tag{83}$$

With $\mathbf{V}$(t) as being the cross sectional velocity and $\mathbf{n}$(t) as the normal vectors.
Furthermore, $V_{max}(t)$ is defined as:

$$V_{max}(t) = max[\mathbf{V}(t) \cdot \mathbf{n}(t)] \tag{84}$$

The pulsatility index for veins (PIV) during a cardiac cycle is defined as

$$PIV = \frac{max(V_{max}) - min(V_{max})}{V_{mean}} \tag{85}$$

where $\max(V_{max})$ is the peak velocity during ventricular systole and $\min(V_{max})$ is the minimum velocity during atrial contraction [15]

Initial Geometry

The geometry of the IUV, DV and LPV are all modelled as straight tubes. However, a more presentable geometry would be to include, in particular, the dilation of DV. Nevertheless, the velocity profile shape is not correctly demonstrated in the 1D model compared to 3D structure. And the results appearing from the model would not be comparable to the literature. Furthermore, the connection of the three vessels are separated with a branch angle α. The wall thickness of the umbilical vein, left portal vein and the ductus venosus are calculated by the ratio equal to $D/h = 11$, $D/h = 11$ and $D/h = 6$. It should be noted that the ductus venosus diameter has been approximated by the valus of the inlet. In addition, several junctions are neglected in this current study that are present in the fetus circulation.

The Youngs modulus and pulse wave velocity in Test 1, see table 4, and in Test 2, see table 5 are obtained by the Moens Koertweg equation [21] that is defined as

$$c = \sqrt{\frac{Eh}{2r\rho}} \tag{86}$$

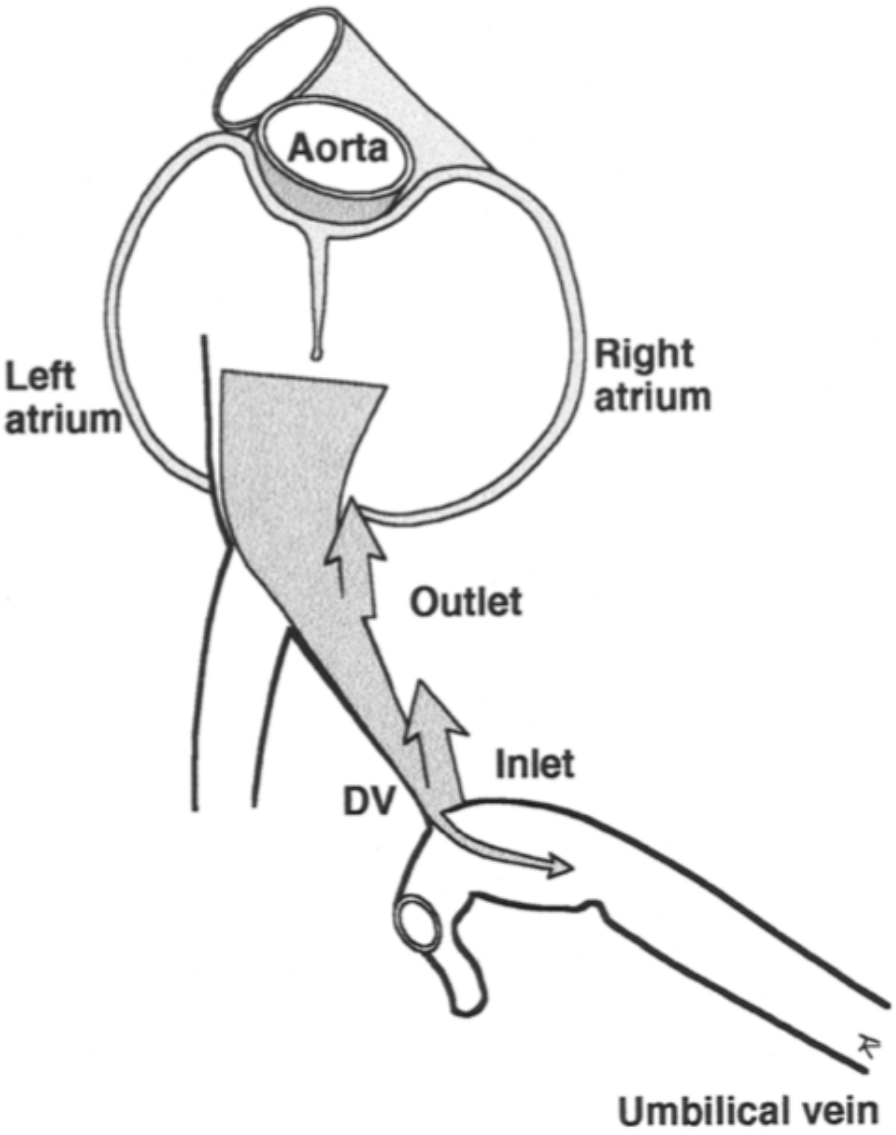

Figure 16: the inferior vena cava,ductus venosus and umbilical vein acting as a transmission line for the pulse wave generated in the atrium. The picture is taken from [30]

Lumped Models

As explained in section 3.1 the lumped models are implemented in order to describe the resistance occurring at the inlet and outlet of each vessel. The DV and LPV are modelled with a three element windkessel (3WK) at each outlet. At DV it represents the part of the Inferior Vena Cava (IVC) that connects the DV to the right atrium. At LPV the 3WK represents the left liver lobe. The 3WK contains of a lumped resistance R, a lumped compliance C and a characteristic impedance Z_c. The UV is modelled with a $\mathcal{L}$ at the inlet with an impedance and compliance. The 3WKs models are determined by the differential equation

$$\frac{dP}{dt} + \frac{(P - P_0)}{R_c C} = Z_c \frac{dQ}{dt} + Q \frac{dZ_c}{dt} + Q \left(\frac{1}{C} + \frac{Z_c}{R_c} C \right), \tag{87}$$

the $\mathcal{L}$ - network is determined by the differential equation

$$\frac{dP}{dt} = -Z_c \frac{dQ}{dt} - Q \frac{dZ_c}{dt} + \frac{(Q_0 - Q)}{C}, \tag{88}$$

where P = P(t) and Q = Q(t) are the pressure and volumetric flow rate at the 1D fluid domain terminals. The pressure source $P_0 = P_0(t)$ is used as a force term for the LPV 3WK model. As it regards the $\mathcal{L}$ network compartment that represent the UV, the flow is introduced by $Q_0 = Q_0(t)$ which is the volumetric flow established at the UV coming from the placenta. Furtermore, the characteristic impedance is defined as

$Z_c = \frac{\rho_f}{A} c(P), (89)$
where c(P) is the pulse wave velocity.

8 Parametric Study

In this thesis, the various geometries regarding ductus venosus, umbilical and left portal vein have been taken from Haugen et al. [18], where the various diameter dimensions were estimated to be 6.1(4.9, 7.1), 1.6(1.1, 2,2) and 3.5(2.6, 4.3) for the umbilical vein, ductus venosus and left portal vein respectively.

Firstly, two tests were investigated with the aim of flow distribution through LPV and DV. The diameters, wall thickness and young modulus were varied in 7 cases. In test 1. the young modulus and wall thickness were calculated from the Moens Koertweg equation and the wall thickness estimated by D/H = 11,6 and 11 for UV,DV and LPV respectively. In test 2, the young modulus were approximately reduced by a factor 2 and the wall thickness were set constant, having a D/H ratio = 10 for all vessels.

Examining the reason for an abnormal wave in ductus venosus, 9 cases were established.

Furtermore, simulations were performed by looking at the pulsations occurring in the three vessels. 7 cases were established and can be found in table 7. It must be stated that these 7 cases are not completely alike the ones in the test 1 4 and test 2 5.

In addition to deterministic modelling, a transformation into stochastic modelling has been applied, which gives rise to a sensitivity analysis. Moreover, the effect and influence on flow due to uncertain parameters will be discussed.

At last, an extension of the umbilical vein were performed, increasing the length and increasing the compliance This gives rise to investigate the connection between the intra abdominal vein and the part outside the fetus.

The following simulations have been carried out:

- 2 tests to assess the flow distribution through LPV and DV.
- 9 cases investigating reason for an abnormal a-wave in DV.
- 7 cases with the interest of pulsations in the UV,DV and LPV.
- 4 Numbers where stochastic modelling have been applied.

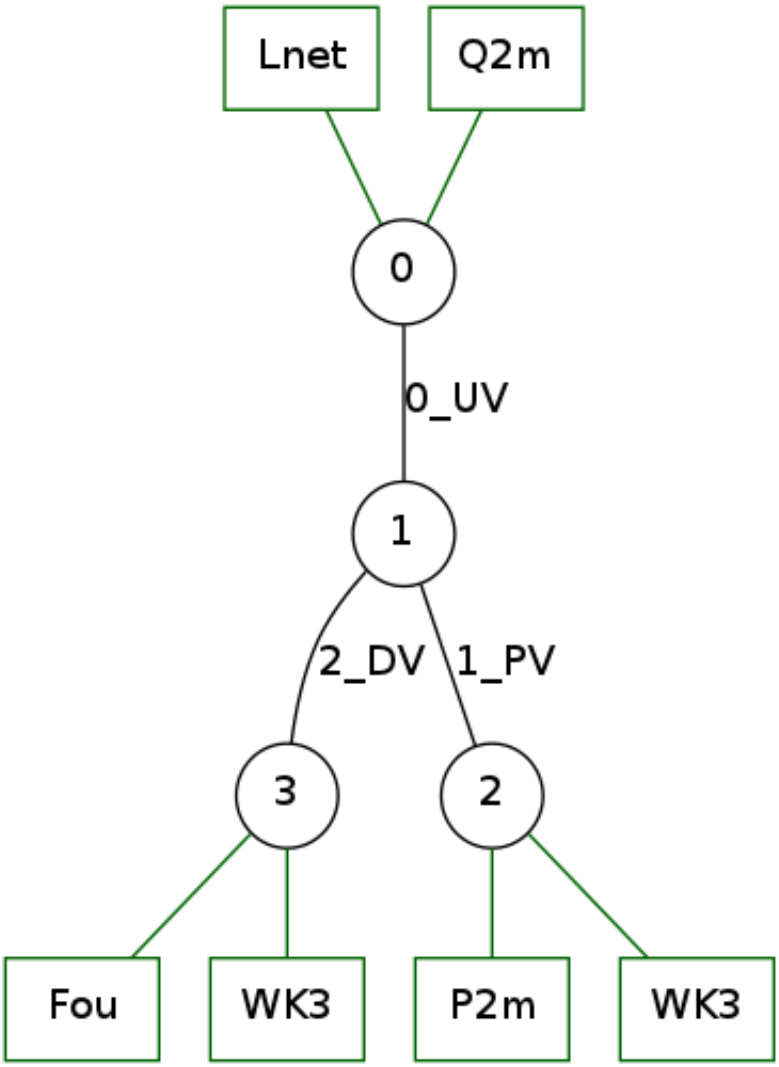

Figure 17: Illustration of the network applied for all the simulations

Where the boundary conditions are presented below:

- Q2m = Applied flow
- Lnet = $\mathcal{L}$ network including an input impedance Z and a compliance C
- Fou = Pulsatile pressure, see equation 81.
- WK3 = Three element windkessel network including a resistance R, characteristic impedance Z, and a compliance C, see section 3.1.3 for more in depth explanation
- P2m = Applied pressure

Material and simulation set up				
Parameter	UV	LPV	DV	
Δx	1.25	0.9375	1.25	
N(grid nodes)	28	8	10	
L	35	7.5	12.5	[mm]

Table 1: Material and simulation set up, applied for the simulations

Global parameters	
Blood density ρ	1060 $[Kg/m^3]$
Blood viscosity μ	0.004 $[Paa]$
CFL number	0.75
Total time T	6.0 $[s]$

Table 2: Global parameters applied for the simulations

Where CFL is defined as:

$$CFL \approx c\frac{\Delta}{t}\Delta x, \tag{90}$$

where c has been calculated by the Bramwell-Hill equation, see equation 8.
With this condition the time step Δt is calculated for each simulation, as the wave speed varies.
The Windkessel and $\mathcal{L}$ boundary condition parameters applied are illustrated in table 3.

Boundary conditions		
Compartment	$R_c\left(\frac{mmHgs}{ml}\right)$	C$\left(\frac{ml}{mmHg}\right)$
UV		0.3
IVC	0.04	0.4
He	0.16	3.0

Table 3: boundary conditions

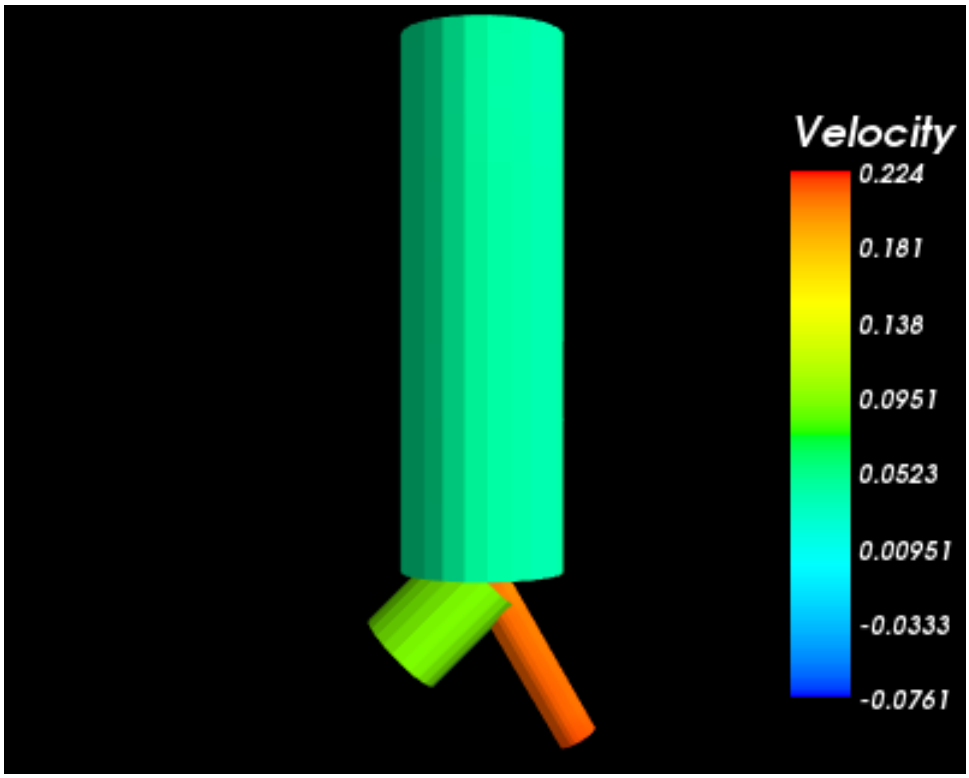

Figure 18: Velocities in the various vessels

8.1 Results

In this section, the results of the simulations, described in *Parametric Study* will be presented. The results will be further discussed in the *Discussion*. See section 9.

8.1.1 The Degree of Shunting Through LPV and DV

In the following, two tests have been established (Test 1 and Test 2). The flow distribution has been of interest in the region of LPV and DV in particular. As mentioned in section 3, how the flow is shunted may come as an indication of various diseases. It is therefore of high significance to establish reasons for how the flow prefer one vessel or another. Test 1 can be found in table 4, and test 2 can be found in table 5. In both tables, a description of the various geometries and material parameters are established. Moreover, the simulation results are also presented where the volume flow and mean velocity have been investigated.

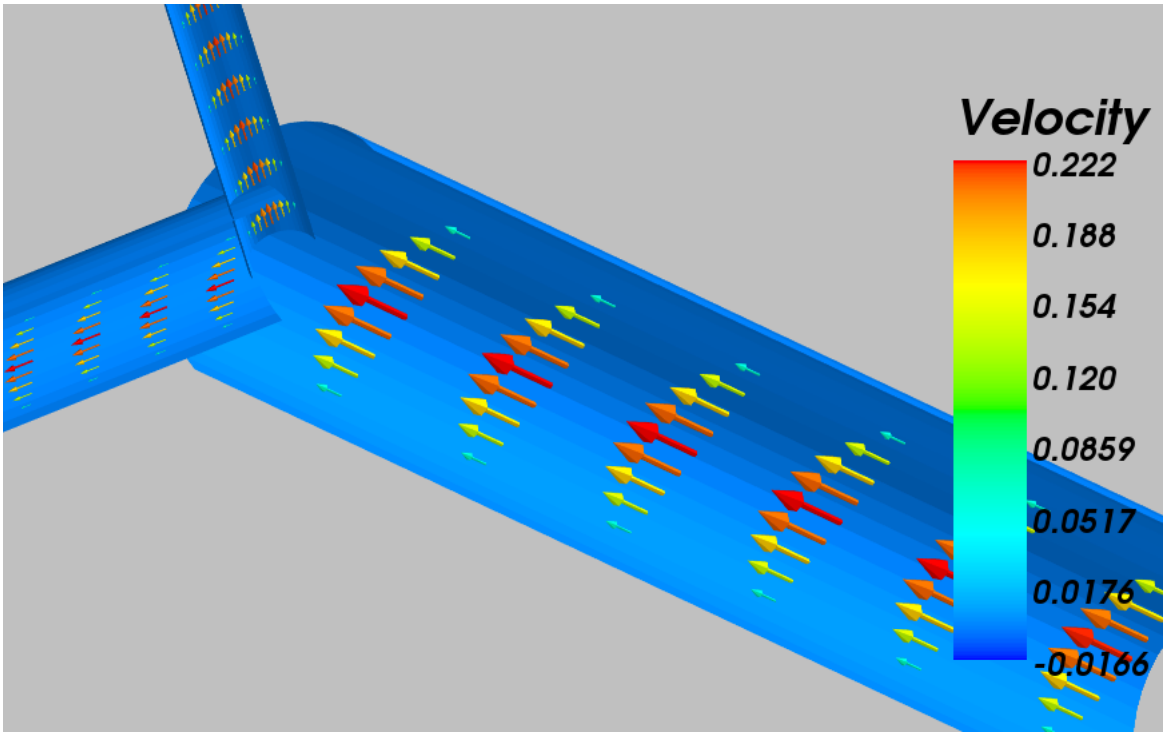

Figure 19: Blood flow in the blood vessels

Table 4: Test 1

Case	1	2	3	4	5	6	7	
D_{DV}	2.2	1.6	1.1	1.6	1.6	1.6	1.6	[mm]
D_{LPV}	3.5	3.5	3.5	3.5	3.5	2.6	4.3	[mm]
D_{UV}	4.9	4.9	4.9	6.1	7.1	6.1	6.1	[mm]
H_{DV}	0.367	0.267	0.183	0.267	0.267	0.267	0.267	[mm]
H_{LPV}	0.318	0.318	0.318	0.318	0.318	0.236	0.39	[mm]
H_{UV}	0.445	0.445	0.445	0.554	0.645	0.554	0.554	[mm]
E_{DV}	19459	19475	19481	19475	19475	19475	19475	$[Pa]$
E_{LPV}	35729	35729	35729	35729	35729	35763	35792	$[Pa]$
E_{UV}	35745	35745	35745	35708	35733	35708	35708	$[Pa]$
Q_{DV}	57.5	32.5	14.4	32.8	32.8	39.3	29.6	$[mL/min]$
Q_{LPV}	37.9	61.43	80.8	63.1	63.1	55.0	66.6	$[mL/min]$
Q_{UV}	95.5	94.1	95.3	95.9	95.9	94.5	96.3	$[ml/min]$
$Q_{DV/UV}$	60.2	34.5	15.1	34.2	34.2	41.6	30.7	%
c_{DV}	1.75	1.75	1.75	1.75	1.75	1.75	1.75	$[m/s]$
c_{LPV}	1.75	1.75	1.75	1.75	1.75	1.75	1.75	$[m/s]$
c_{UV}	1.75	1.75	1.75	1.75	1.75	1.75	1.75	$[m/s]$
V_{DVmean}	20.6	23.5	14.4	21.8	21.8	25.3	19.9	$[cm/s]$
$V_{LPVmean}$	5.4	8.5	10.9	8.7	8.7	13.4	6.2	$[cm/s]$
V_{UVmean}	6.8	6.6	6.6	4.4	3.2	4.2	4.4	$[cm/s]$

Table 5: Test2

Case	1	2	3	4	5	6	7	
D_{DV}	2.2	1.6	1.1	1.6	1.6	1.6	1.6	[mm]
D_{LPV}	3.5	3.5	3.5	3.5	3.5	2.6	4.3	[mm]
D_{UV}	4.9	4.9	4.9	6.1	7.1	6.1	6.1	[mm]
H_{DV}	0.22	0.16	0.11	0.16	0.16	0.16	0.16	[mm]
H_{LPV}	0.35	0.35	0.35	0.35	0.35	0.26	0.43	[mm]
H_{UV}	0.49	0.49	0.49	0.61	0.71	0.61	0.61	[mm]
E_{DV}	10477	10477	10477	10477	10477	10477	10477	[Pa]
E_{LPV}	17500	17500	17500	17500	17500	17500	17500	[Pa]
E_{UV}	17500	17500	17500	17500	17500	17500	17500	[Pa]
Q_{DV}	85.7	50.9	22.8	50.8	50.8	56.9	47.8	$[mL/min]$
Q_{LPV}	10.8	45.4	73.2	45.5	45.5	38.9	48.6	$[mL/min]$
Q_{UV}	96.5	96.3	96.1	96.4	96.4	96.1	96.5	$[ml/min]$
$Q_{DV/UV}$	88.8	52.9	23.7	52.7	52.7	59.2	49.5	%
c_{DV}	0.99	0.99	0.99	0.99	0.99	0.99	0.99	$[m/s]$
c_{LPV}	1.28	1.28	1.28	1.28	1.28	1.28	1.28	$[m/s]$
c_{UV}	1.28		1.28	1.28	1.28	1.28	1.28	$[m/s]$
V_{DVmean}	23.3	24.6	22.1	24.6	24.5	26.6	23.5	$[cm/s]$
$V_{LPVmean}$	1.3	5.5	8.6	5.5	5.5	8.4	3.9	$[cm/s]$
V_{UVmean}	6.0	5.9	5.7	3.8	2.8	3.7	3.9	$[cm/s]$

8.1.2 Abnormal flow in Ductus Venosus

9 test cases were established in order to investigate reasons for the reversed flow during atrial contraction in the ductus venosus. The atrial contraction wave is a poor clinical sign in fetal diseases discussed in section 3.
Under normal pregnancies, during ventricular systole, the waveform is recognized as a maximum peak. During diastolic filling, a second peak is observed. A strong velocity reduction is often observed during atrial contraction and may occasionally come out as a flow reversal. However, reversed flow is related to a healthy fetus in the first trimester of gestation, yet it is abnormal in later stages of gestation. In the following, the parametric set up and the results are demonstrated.

Table 6: Parametric study aiming at velocity pulsations in the ductus venosus

Case	1	2	3	4	5	6	7	8	9	
$P_{0,He}$	3.3	3.3	3.3	4.3	4.3	4.3	4.3	4.3	4.3	[mmHg]
$P_{0,IVC}$	1.4	1.4	1.4	1.4	1.4	1.4	2.8	2.8	2.8	[mmHg]
$P_{A,IVC}$	4.5	3.0	1.5	1.5	3.0	4.5	1.5	3.0	4.5	[mmHg]
D_{UV}	6.1	6.1	6.1	6.1	6.1	6.1	6.1	6.1	6.1	[mm]
D_{DV}	1.6	1.6	1.6	1.6	1.6	1.6	1.6	1.6	1.6	[mm]
D_{LPV}	3.5	3.5	3.5	3.5	3.5	3.5	3.5	3.5	3.5	[mm]
H_{UV}	0.61	0.61	0.61	0.61	0.61	0.61	0.61	0.61	0.61	[mm]
H_{DV}	0.16	0.16	0.16	0.16	0.16	0.16	0.16	0.16	0.16	[mm]
H_{LPV}	0.35	0.35	0.35	0.35	0.35	0.35	0.35	0.35	0.35	[mm]
E_{UV}	17500	17500	17500	17500	17500	17500	17500	17500	17500	$[Pa]$
E_{DV}	10477	10477	10477	10477	10477	10477	10477	10477	10477	$[Pa]$
E_{LPV}	17500	17500	17500	17500	17500	17500	17500	17500	17500	$[Pa]$
PI_{DV}	7.23	2.65	1.01	0.68	1.98	4.64	1.16	3.5	11.6	
Q_{DV}	15.5	27.2	34.9	45.9	38.4	27.1	33.5	25.1	12.4	$[mL/min]$
Q_{LPV}	79.6	68.8	61.5	50.4	57.5	68.1	62.8	70.8	82.7	$[mL/min]$

Table 6 supports Matias et al. [12] statement that the pulsatility index(PI) is significantly higher for chromosomally abnormal fetuses. The PI for chromosomally normal fetuses were found to be in the range of 0.6-3.3, whereas for chromosomally abnormal fetuses in the range of 0.8 - 7.7. In addition, the median heights of the S and D waves (waves during systole and diastole) were discovered to be significantly lower, and are demonstrated in figures 20 and 21 for the cases 1,6 and 9. Furthermore, cases 1,6 and 9 also represents the most abnormal flow during atrial contraction due to high velocity reversal.

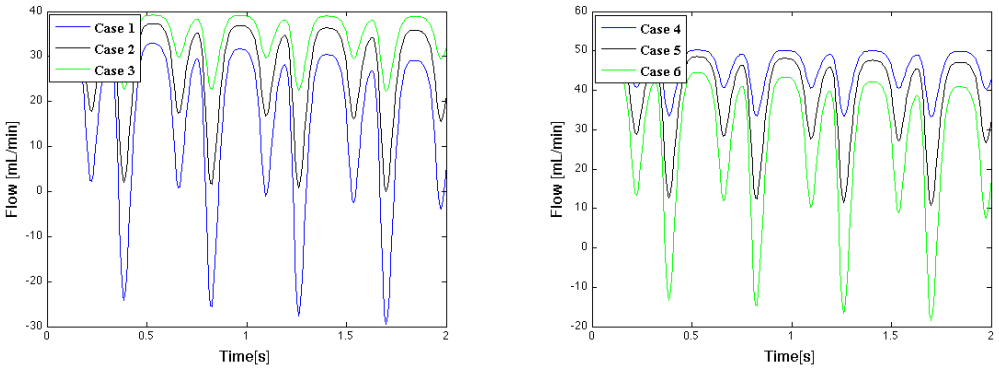

Figure 20: Abnormal flow in DV, case 1-6

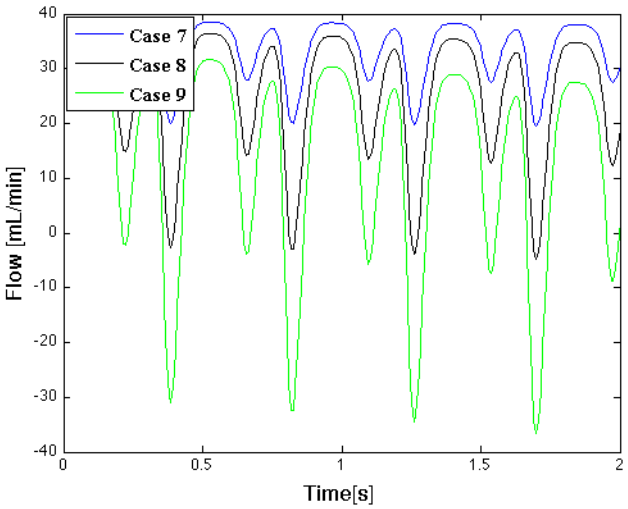

Figure 21: Abnormal flow in DV, case 7-9

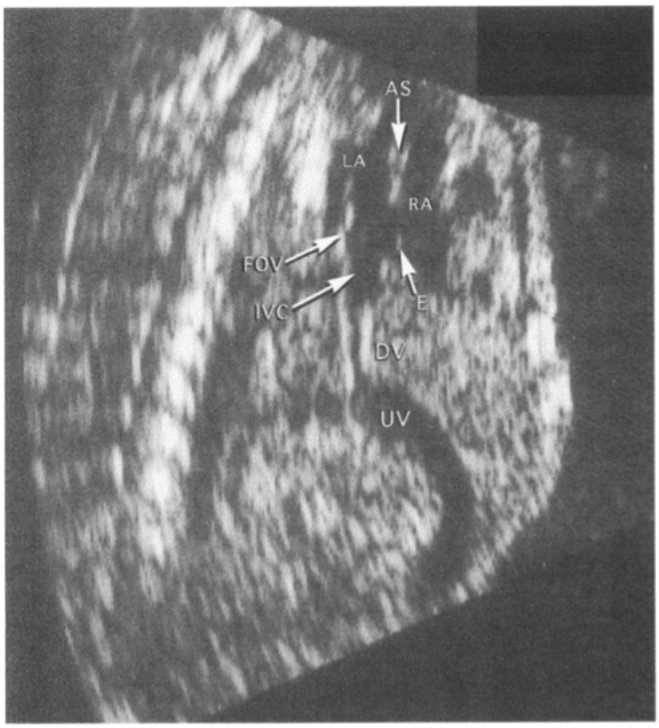

Figure 22: An ultrasound scan of a normal fetus at 30 weeks of gestation illustrating the ductus venosus connecting the umbilical vein to the inferior vena cava. Taken from [30]

8.1.3 Pulsatile flow

Pulsatile flow has been investigated by means of 7 cases varying only the diameters of UV, LPV and DV. Firstly, the simulations with an altered DV diameter is established. Secondly, an altered UV diameter is established. At last, the LPV diameter is varied. Moreover, in order to compare the pulsatile flow due to geometry variations, the figures will be presented in case 1 to 7 for each vessel.

Table 7: Geometries

Case	1	2	3	4	5	6	7	
D_{UV}	6.1	6.1	6.1	4.9	7.1	6.1	6.1	[mm]
D_{PV}	3.5	3.5	3.5	3.5	3.5	2.6	4.3	[mm]
D_{DV}	2.2	1.6	1.1	1.6	1.6	1.6	1.6	[mm]

Volume flow obtained in the ductus venosus for cases 1 -7

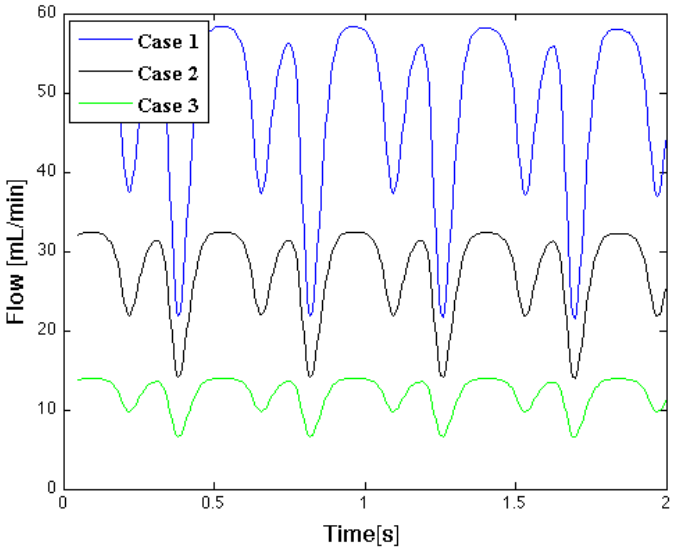

Figure 23: Variation of DV diameter

Figure 23 illustrates the flow in DV were a variation of DV diameters has been applied. Case 1 represents the geometry with the highest DV diameter and therefore the highest volume flow shunted through DV. Contrarily, case 3 represents the geometry with the lowest DV diameter and consequently the lowest flow shunted through DV. In addition, the pulsatile flow show a clear dependency on the DV diameter, whereas high diameter provide high pulsations.

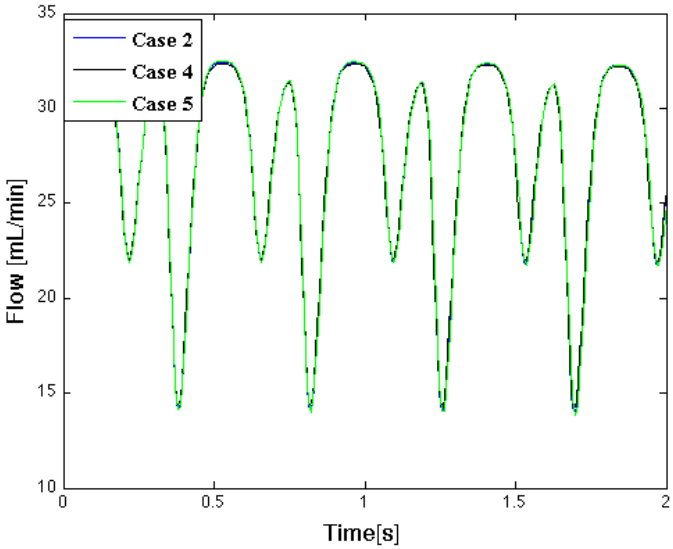

Figure 24: Variation of UV diameter

Figure 24 illustrates the flow in DV were a variation of UV diameters has been applied. However, in contrast to the flow in figure 23, a neglected variation is observed.

Consequently, the UV diameter does not affect the flow pattern in DV.

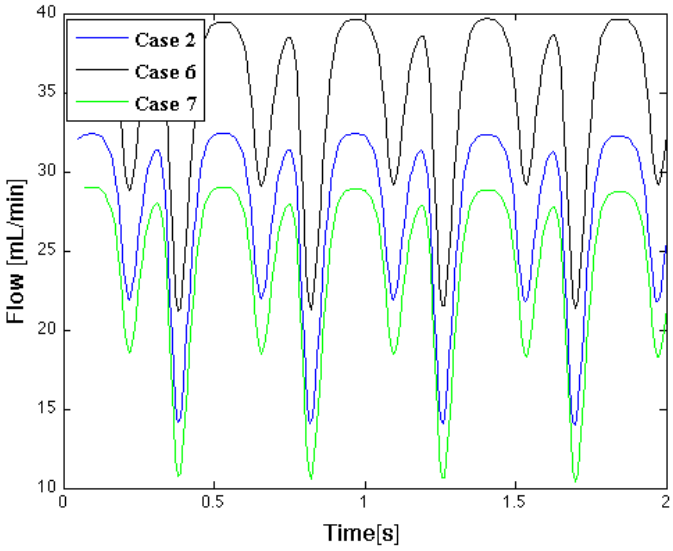

Figure 25: Variation of LPV diameter

Figure 25 also illustrates the flow in DV, yet with a variation of LPV diameter. A more significant difference than in figure 24 is observed. The flow pulsations are less affected. However, the degree of shunting shows clear dependency on the LPV diameter. Thus, the degree of shunting through DV decreases as the diameter of LPV increases.

Thus, the figures 23, 24 and 25 demonstrate the flows dependency on the diameters of LPV and DV, and less due to the diameter of UV when it comes to pulsations and the degree of shunting through DV. The geometry of DV influences both the pulsations and the degree of shunting through DV, while the geometry of LPV only affect the the degree of shunting through DV.

Volume flow in umbilical vein for cases 1-7

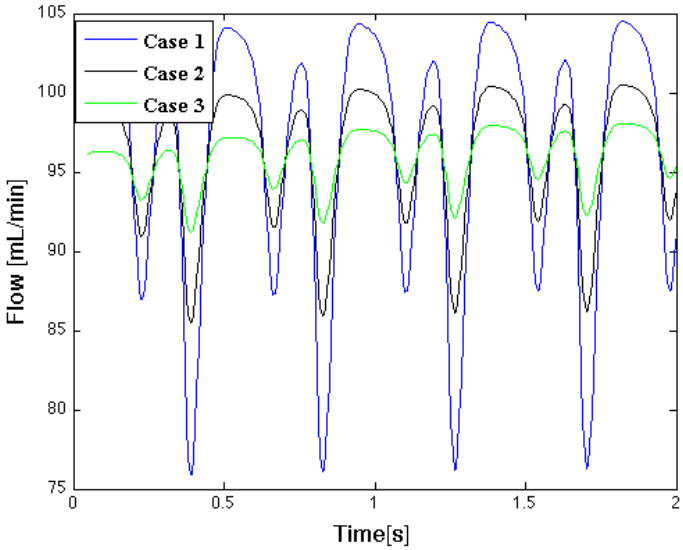

Figure 26: Variation of DV diameter

Figure 26 illustrates the flow in UV where a variation of DV diameters has been applied. Case 1 represents the flow with the highest DV diameter and is consequently the case with the highest pulsations. Moreover, the pulsations are significantly higher than for case 2 and 3, where the diameters in DV decrease.

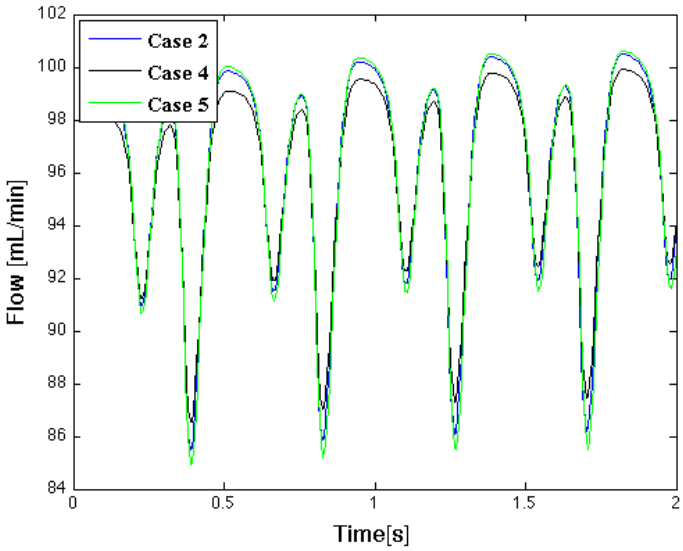

Figure 27: Variation of UV diameter

Figure 27 illustrates the flow in UV where a variation of UV diameters has been applied. It is observed that the pulsations are less dependent on the diameter of UV.

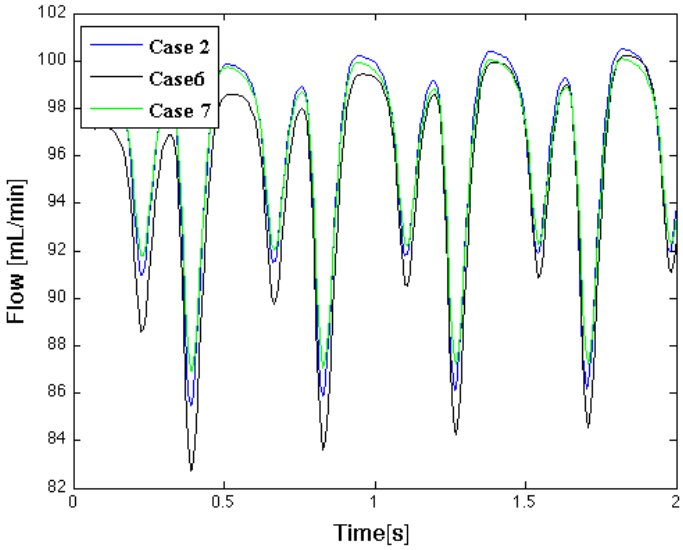

Figure 28: Variation of LPV diameter

Figure 28 illustrates the flow in UV where a variation of LPV diameters has been applied. The same observation as in figure 27 is detected, where the pulsations show less variety.

Thus, the figures 26, 27 and 28 demonstrate that the pulsatile flow in UV is strongly dependent on the diameter of DV.

Volume flow in Left Portal vein for cases 1-7

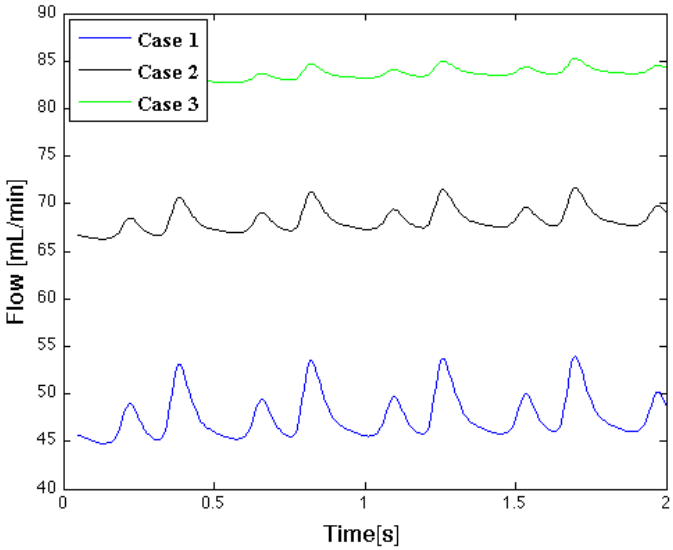

Figure 29: Variation of DV diameter

Figure 29 illustrates the flow in LPV where a variation of DV diameters has been applied. The figure clearly demonstrates the flows dependency on DV diameters where pulsations are high at high DV diameter and smaller at low DV diameter. In addition, the degree of shunting through LPV due to DV diameter is significant. The figure shows clearly a correlation between the degree of shunting and DV diameter. Case 3 involves the geometry with the smallest diameter of DV. As a result, the highest volume flow in LPV is obtained. In contrast, case 1 has the highest DV diameter and represents the lowest degree of shunting through LPV.

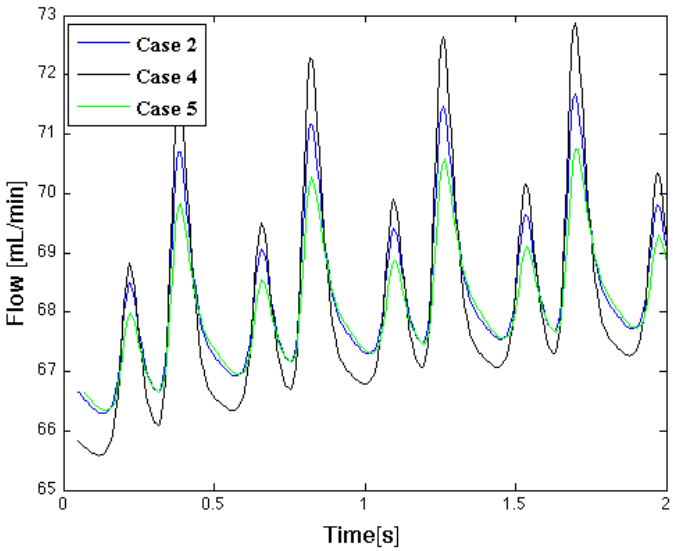

Figure 30: Variation of UV diameter

Figure 30 illustrates the flow in LPV where a variation of UV diameters has been applied. The pulsations show less influence by UV diameter alteration, however, the pulsations do increase at decreasing values of the UV diameter. This is explained by the pulsatile pressure applied at the IVC compartment at the outlet of DV, causing a pulsatile flow in the positive direction of LPV. Thus, the pulsatile flow distribution between UV and LPV is dependant on the UV/LPV diameter ratio, whereas small UV diameters forces pulsatile flow into LPV.

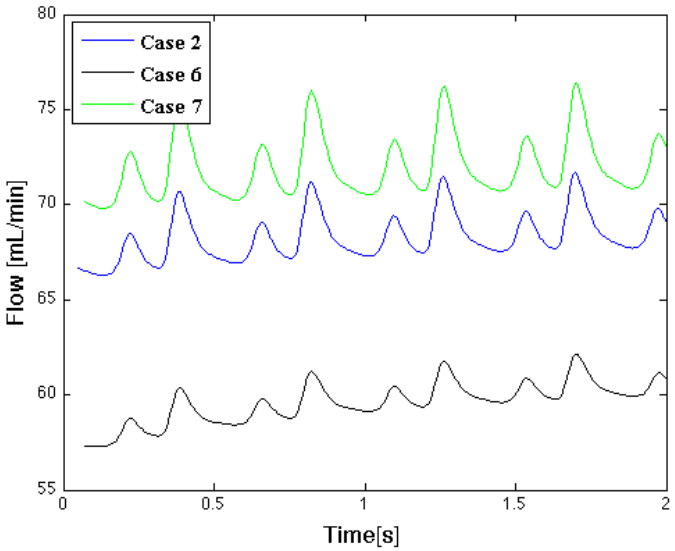

Figure 31: Variation of LPV diameter

Figure 31 illustrates the flow in LPV where a variation of LPV diameters has been applied. The flow pulsations do not vary as much as in the cases 1,2 and 3, see figure 29 where the DV diameter was varied. Nevertheless, visible differences are obtained when it comes to the degree of shunting though LPV, whereas high LPV diameter provides high volume flow, see case 7.

Thus, the figures 29, 30 and 31 demonstrate the flows dependency on DV diameter when it comes to pulsations. In addition, UV diameter does also affect the pulsatile flow in LPV yet of minor importance. The diameter of LPV itself does only affect the volume flow shunted through LPV.

8.1.4 Stochastic modelling of the Umbilical Vein, Left Portal Vein and Ductus Venosus

In the following, stochastic simulations where the parameters have been considered uncertain are presented. The various simulations are numbered from 1 to 4. A complete description of the stochastic modelling is given in table 8

Simulations including only an uncertainty in the diameter of both the umbilical vein and the ductus venosus have been established. The impact of an uncertainty in the diameter regarding both umbilical vein and ductus venosus are shown in Number 1.

Simulations having an uncertainty in the ductus venosus diameter, Young modulus and wall thickness have been conducted. This is shown in Number 2. Furthermore, simulations including an uncertainty in the umbilical vein parameters have also been conducted, where the same parameters as for ductus venosus have been investigated. See Number 3 for illustrations.

Not only do the material parameter contribute to an uncertainty of the fetal circulation, but also the boundary conditions. Therefore, simulations regarding the compliance and resistance have been performed. The compliance term in the $\mathcal{L}$ boundary condition represents the placenta, at the inlet of the umbilical vein. The resistance term in the Windkessel boundary condition, at both outlets of LPV and DV represents the He and IVC compartments. The range of uncertainty for the resistance and compliance can be found in Number 4, see table 8.

Table 8: Description of the simulations

Stochastic modelling			
Number	UV	LPV	DV
1	D 4.9-7.1 mm		D 1.1 - 2.2 mm
2			D 1.1 - 2.2 mm E 10477 -19482 Pa H 0.11 - 0.367 mm
3	D 4.9 - 7.1 mm E 17500 - 35745 Pa H 0.445 - 0.71 mm		
4	C 0.1 - 0.3	R 0.16 - 0.32 $mmHg$	R 0.04 0.8 $mmHg$

For all the stochastic simulations, i.e Number 1 - Number 4, the following will be applicable:
To the left, figures showing the mean flow. To the right, STD of the same simulations. Accordingly, the sensitivity of the signals can be measured, since high variation imply high sensitivity.The mean flow represents the expected value i.e. the value that is most likely to occur when simulating with a variety of uncertainties in data. Moreover, "mean UV,DV" is the mean flow due to uncertain parameters regarding UV and DV respectively.

In addition, "mean all" is the mean flow due to uncertain parameters for both UV and DV together. "STD UV, DV" and" STD all" are the standard variations of the same simulation.

Number1

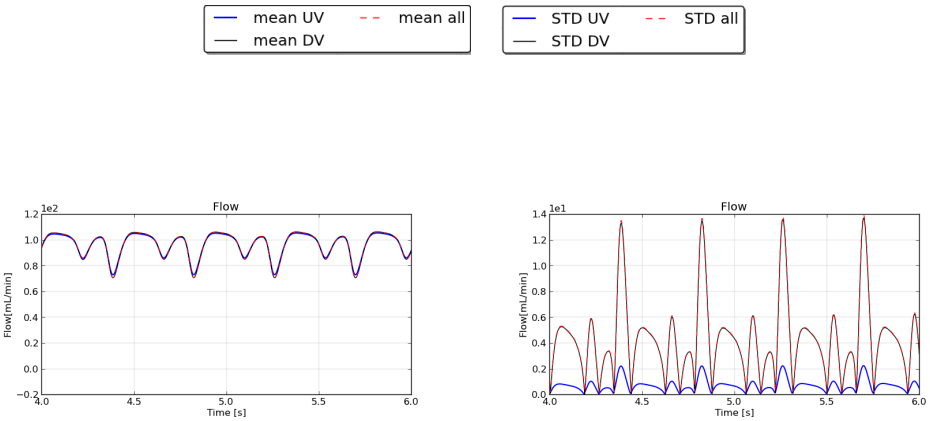

Figure 32: Total blood flow, Umbilical vein

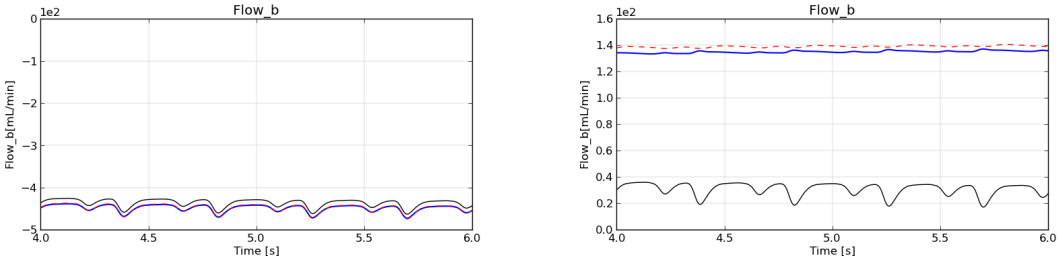

Figure 33: Backward blood flow, Umbilical vein

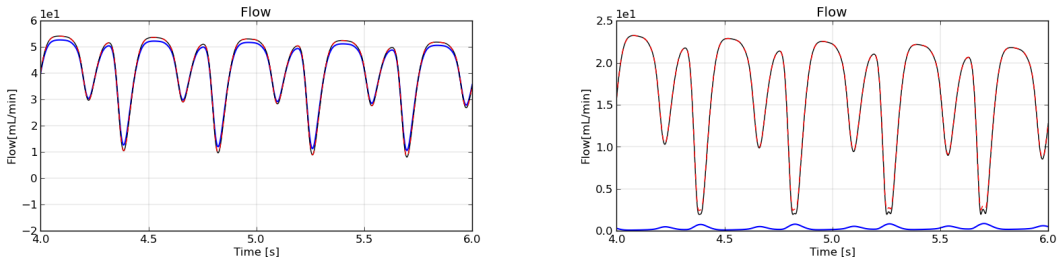

Figure 34: Total blood flow, ductus venosus

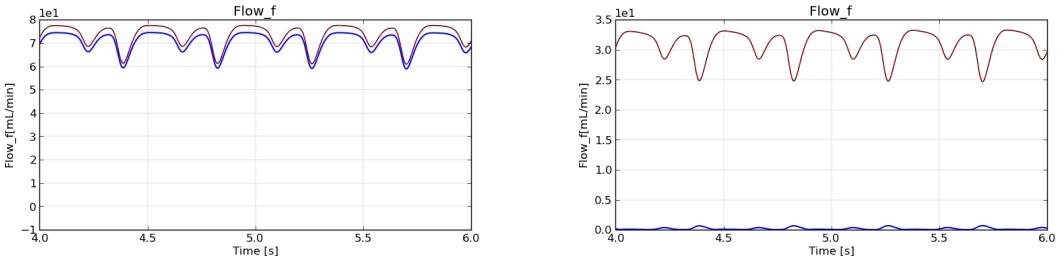

Figure 35: Forward blood flow, ductus venosus

Figure 32 illustrates the mean and STD of the total flow in UV, when an uncertainty of both UV and DV diameters have been applied. Figure 33 illustrates the backward flow in UV for the same simulation. Moreover, the uncertain parameters, i.e diameters of UV and DV, do affect the flow pattern differently, where the total as well as backward flow is strongly sensitive to the DV diameter when it comes to pulsations. The backward flow is sensitive to UV diameter when it comes to the amount transmitted back into UV.

Figure 34 illustrates the mean and STD of the total flow in DV for the same simulation as for the figures above. In addition, figure 35 illustrates the forward flow. The flow is also most sensitive of the DV diameter and minor of the diameter of UV. Moreover, the forward flow demonstrates an almost negligible influence of the uncertainty of UV diameter.

STD of Number1 in time and amplitude

The boxes illustrates the mean and standard deviation with respect to time and amplitude. This is providing knowledge regarding which diameter that influences the peaks within a cardiac cycle. The blue box shows the STD for the vessel that includes an uncertainty in data, the yellow area represent the total STD, the red line represents the mean value and the black dotted line represents the total mean value. The sensitivity of both diameters of UV and DV are illustrated in figures 36 and 37 for both umbilical vein and ductus venosus.

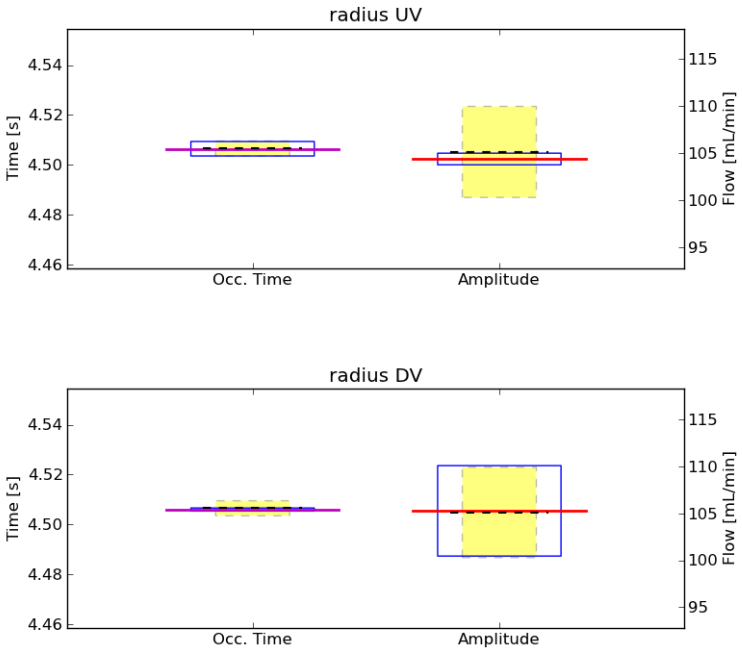

Figure 36: Sensitivity of peak during systole in umbilical vein

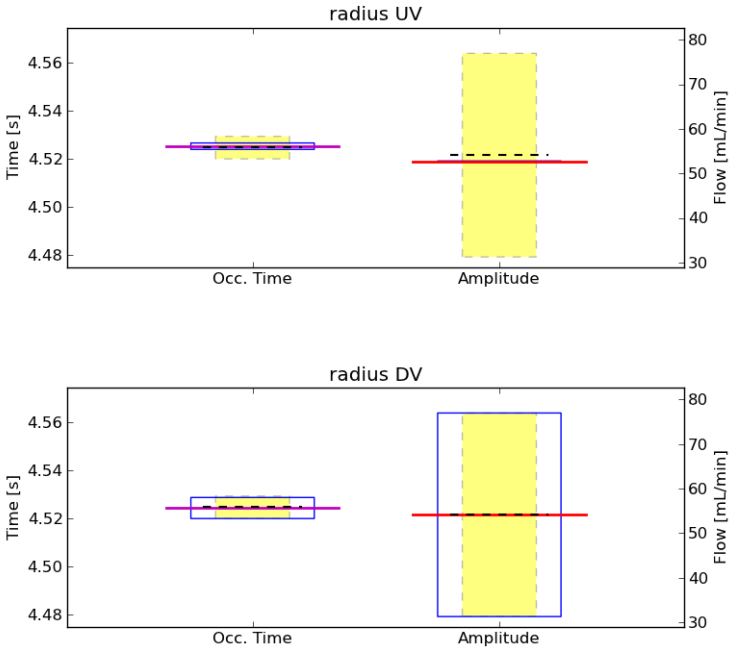

Figure 37: Sensitivity of peak during systole in ductus venosus

The figures 36 and 37 illustrate the sensitivity of peak during systole in the umbilical vein and ductus venosus respectively for simulation Number1. The sensitivity in time is

almost negligible for both vessels, however, the flow amplitudes are clearly sensitive to the uncertain parameters. Nevertheless, it is mainly the uncertainty of DV diameter that influences the flow, whereas a clear response is shown in figure 36 while an even more visible response is shown in figure 37.

Confidence intervals of Number1

The confidence intervals related to the sensitivity of peaks are demonstrated below. The same peak as in the above figures is presented, in addition to the second peak during diastole and the peak during atrial contraction. The figures illustrate that the flow is highly sensitive to the radius of DV and less sensitive to the UV radius. In particular, the peak occurring in DV is sensitive to the radius of DV. See figures 38 and 39.

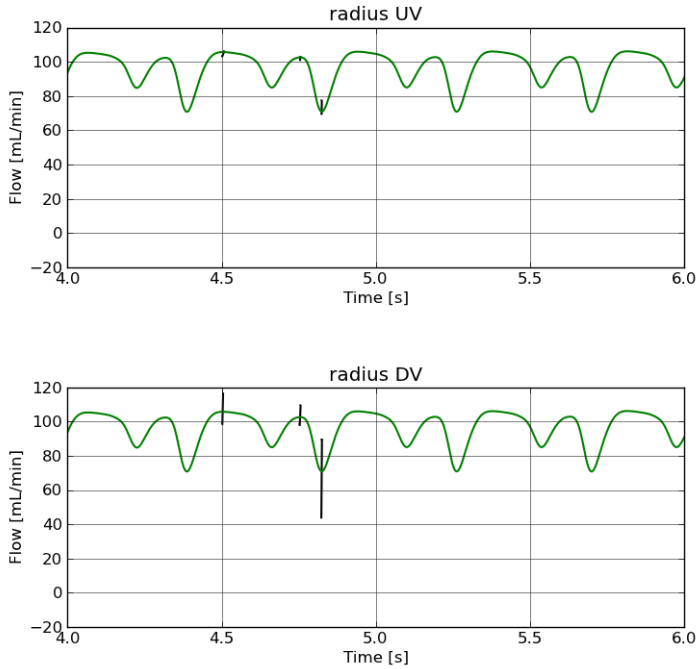

Figure 38: sensitivity of peaks in the umbilical vein

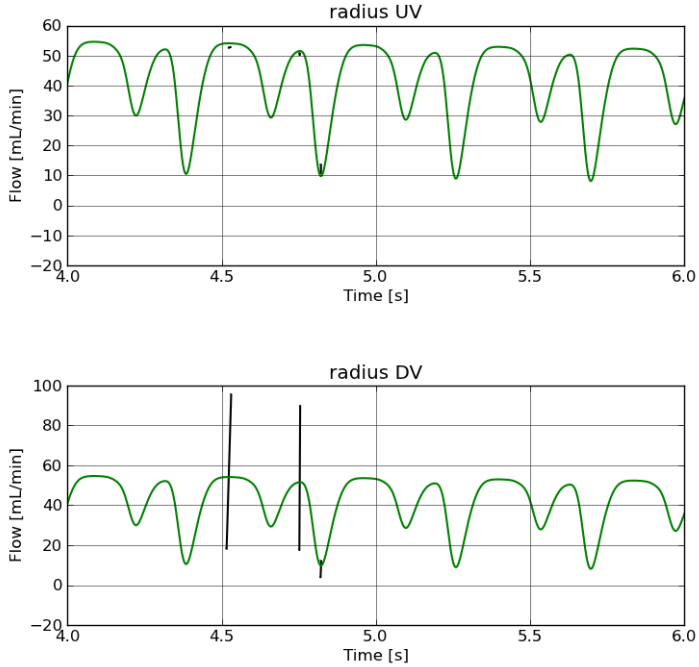

Figure 39: sensitivity of peaks in the ductus venosus

In the following, the uncertain parameters applied in the simulation are the radius, young modulus and wall thickness in the ductus venosus. The results are illustrated in the figures below.

Number2

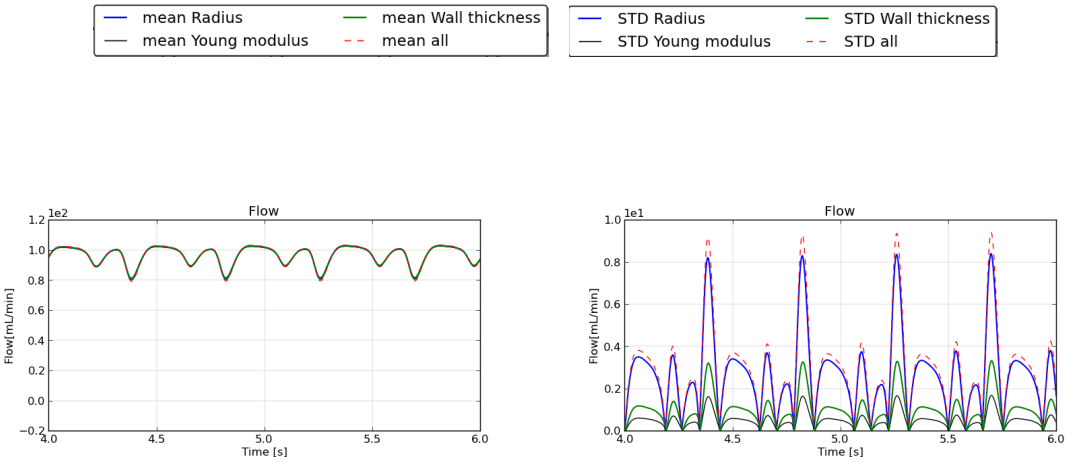

Figure 40: Total blood flow, umbilical vein

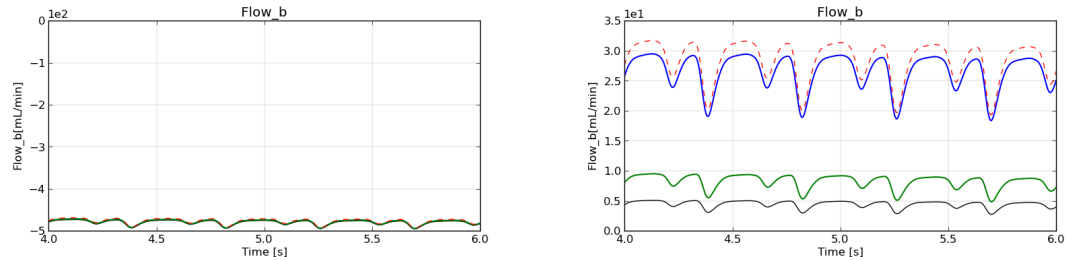

Figure 41: Backward blood flow, umbilical vein

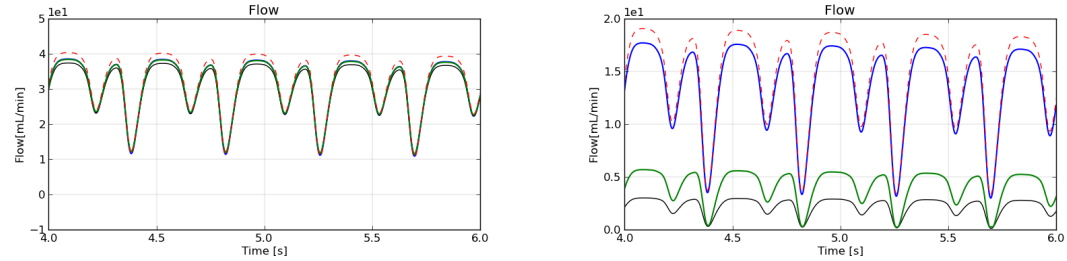

Figure 42: Total blood flow, ductus venosus

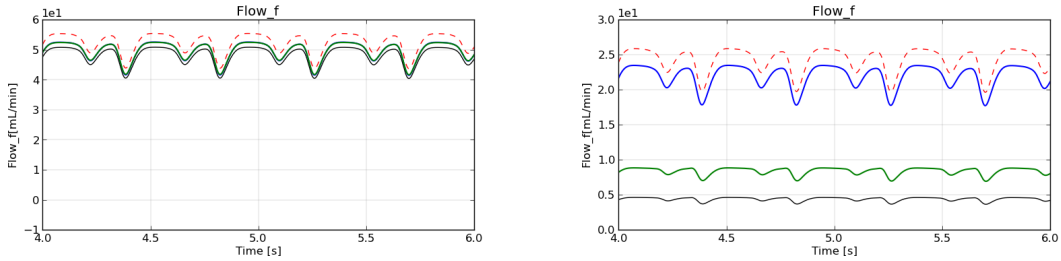

Figure 43: Forward blood flow, ductus venosus

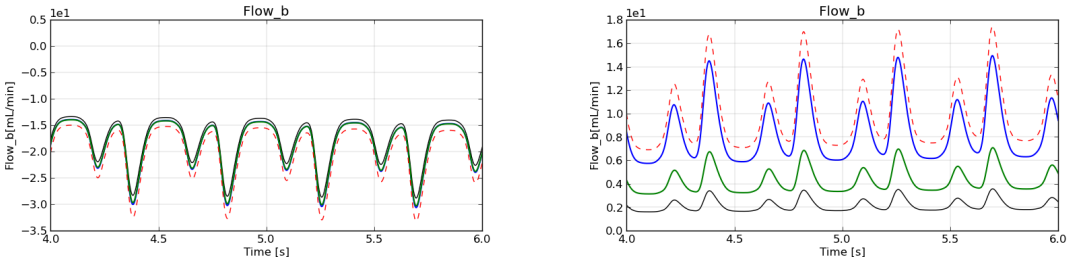

Figure 44: backward blood flow, ductus venosus

Figures 40, 41, 42, 43 and 44 illustrate the flow in umbilical vein and ductus venosus with three uncertain parameters. As already mentioned, these parameters are the radius, young modulus and wall thickness and take place in the ductus venosus. Furthermore, the uncertain parameters influence of the flow pattern are shown in the figures above. In all figures, the parameter that has a great impact of the flow pattern is the radius of DV. Moreover, the young modulus is the second most important parameter, while the wall thickness is of minor significance. In this simulation, it is also clear that the flow flaps in the opposite direction when the flow is propagating against the pressure pulse, see figures 43 and 44 for illustrations.

Confidence interval of Number2

The confidence intervals illustrated in figures 45 and 46 show the peaks appearance at a 99 % confidence level. The lines take place at the peaks during systole, diastole and atrial contraction for both UV and DV. Moreover, the figure states the conclusion above that the radius of DV provides high sensitivity in flow, especially in DV.

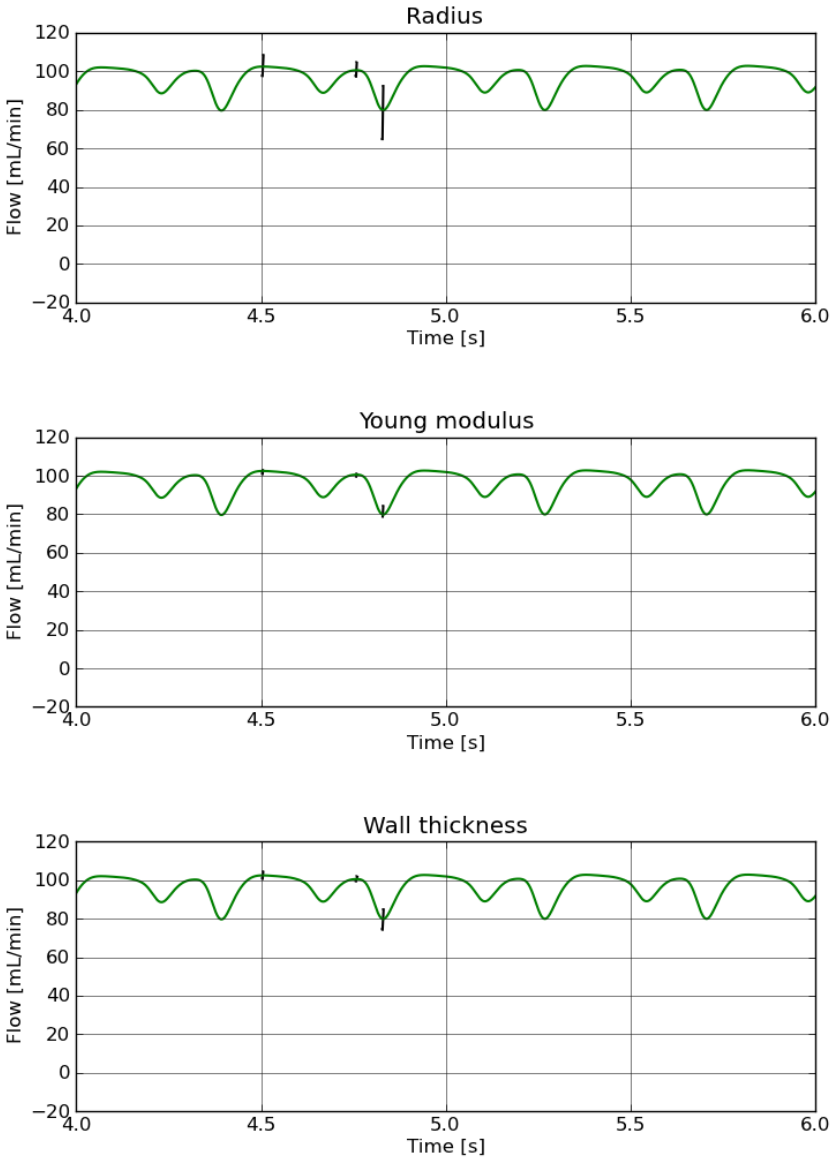

Figure 45: Sensitivity of peaks in umbilical vein

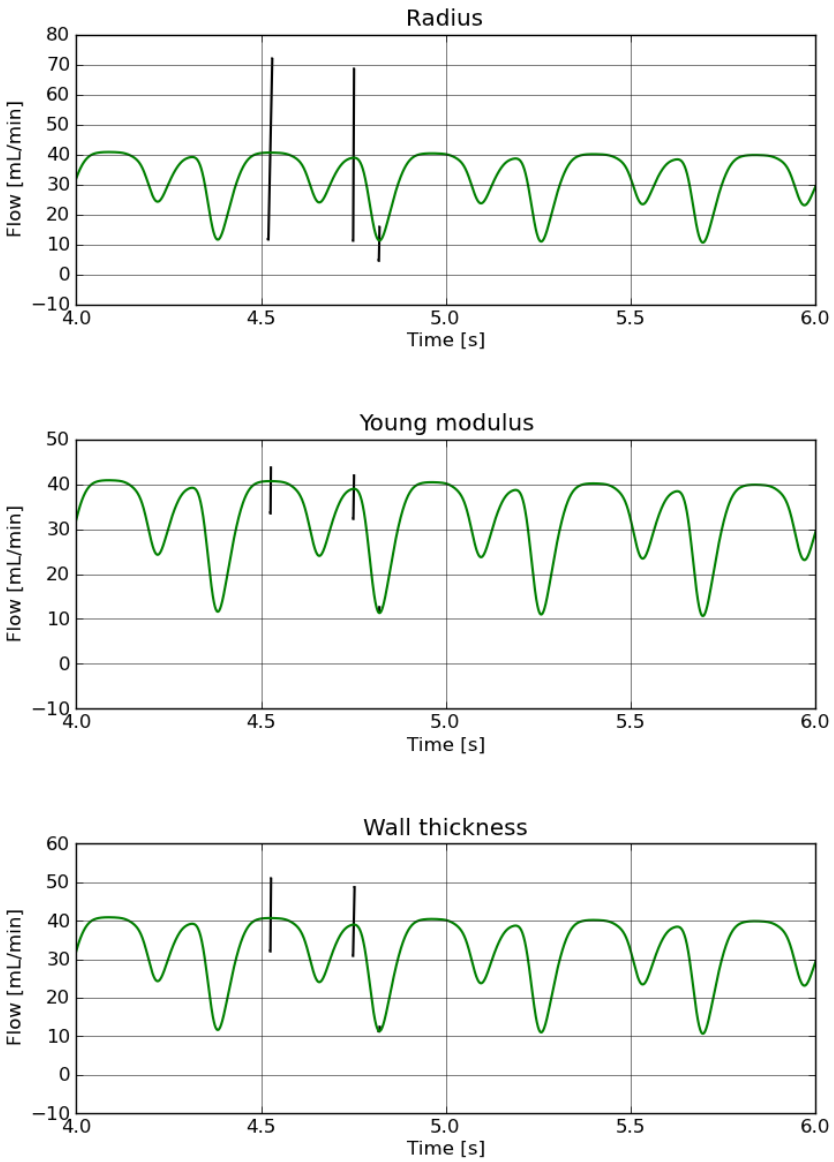

Figure 46: Sensitivity of peaks in ductus venosus

STD of Number2 in time and amplitude

Figure 47 illustrates the sensitivity of peaks due to the uncertain parameters in Number2 where STD box plots have been utilized. As already stated, the radius provide high sensitivity and can be observed in this figure. The yellow box represents the total STD of all the uncertain parameters, the blue box represents the STD due to an uncertainty in the respected parameter. Furthermore, figure 47 illustrates the STD of peak during systole in ductus venosus.

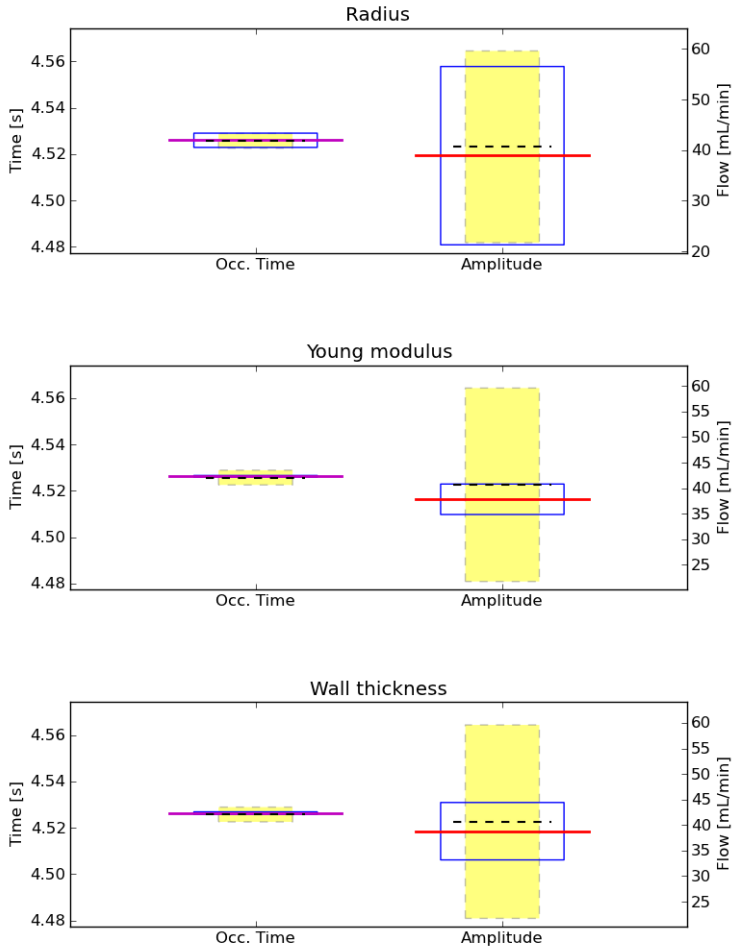

Figure 47: Sensitivity of peak during systole in ductus venosus

Number3:

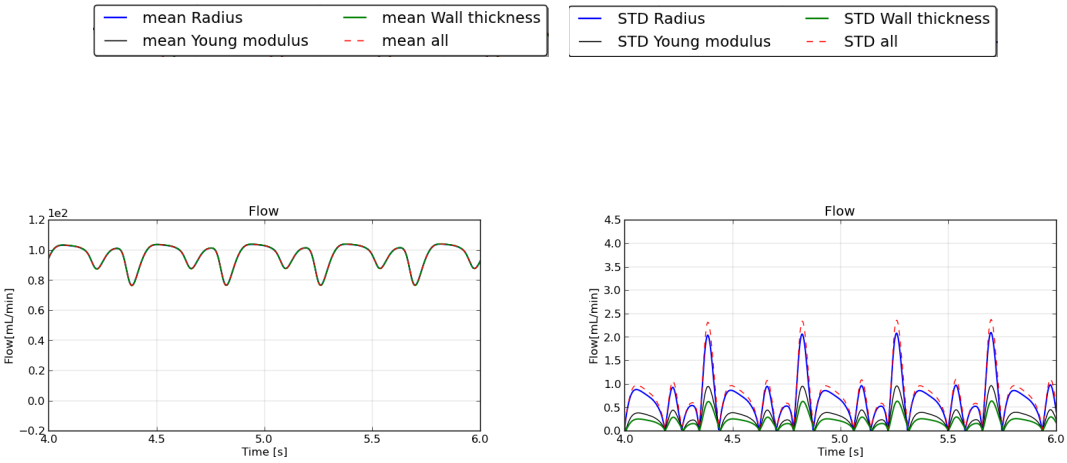

Figure 48: Total blood flow, Umbilical vein

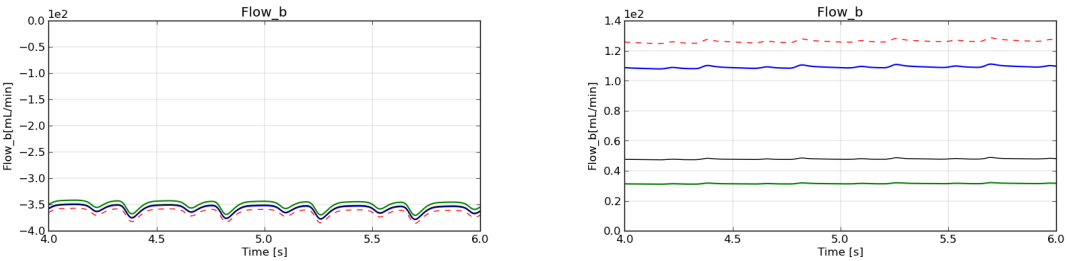

Figure 49: Backward blood flow, Umbilical vein

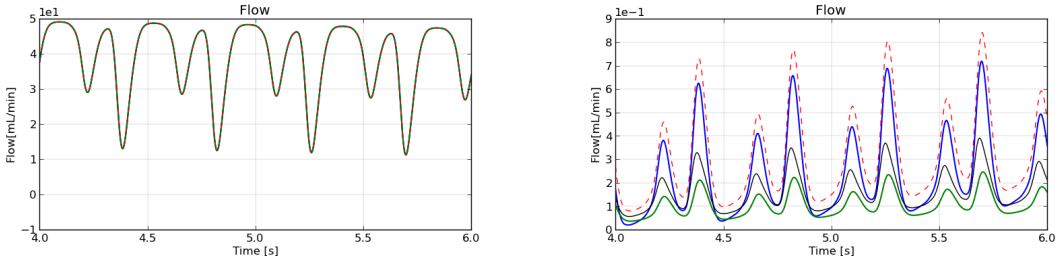

Figure 50: Total blood flow, ductus venosus

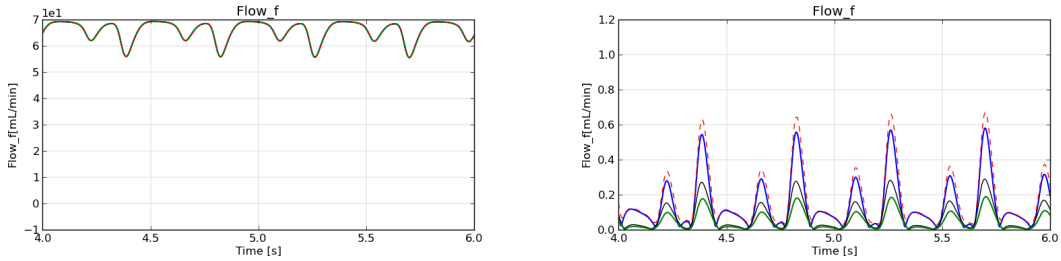

Figure 51: Forward blood flow, ductus venosus

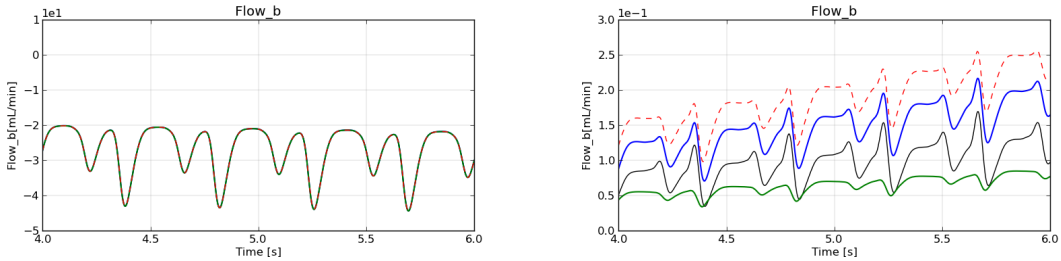

Figure 52: backward blood flow, ductus venosus

In Number3, simulations have been performed including an uncertainty in the same parameters as in Number2, yet the uncertain parameters takes place in the umbilical vein and not ductus venosus. As observed in the figures for Number2, an uncertainty within the parameters of DV provided significant results for both vessels. However, in simulation Number3, the flow pattern in ductus venosus does not seem to be influenced by the uncertain parameters in UV, see figures 50, 51 and 52. (Note, the y-axis is different than in Number2). Moreover, the backward flow in UV shows minor sensitivity in pulsations due to an uncertainty in parameters of UV itself, see figure 49. Figure 48, where the total flow in UV is shown, illustrates that the flow pattern is not as sensitive to the uncertainty in UV parameters as for DV parameters.

Confidence interval of Number3

Figures 53 and 54 illustrate the confidence intervals in both UV and DV showing the prediction of the peaks appearance with a 99 % confidence. It is observed by the figures that the flow impact due to the parameters applied in the simulation are of minor importance for both UV and DV. STD box plots of this simulation will therefore not be presented.

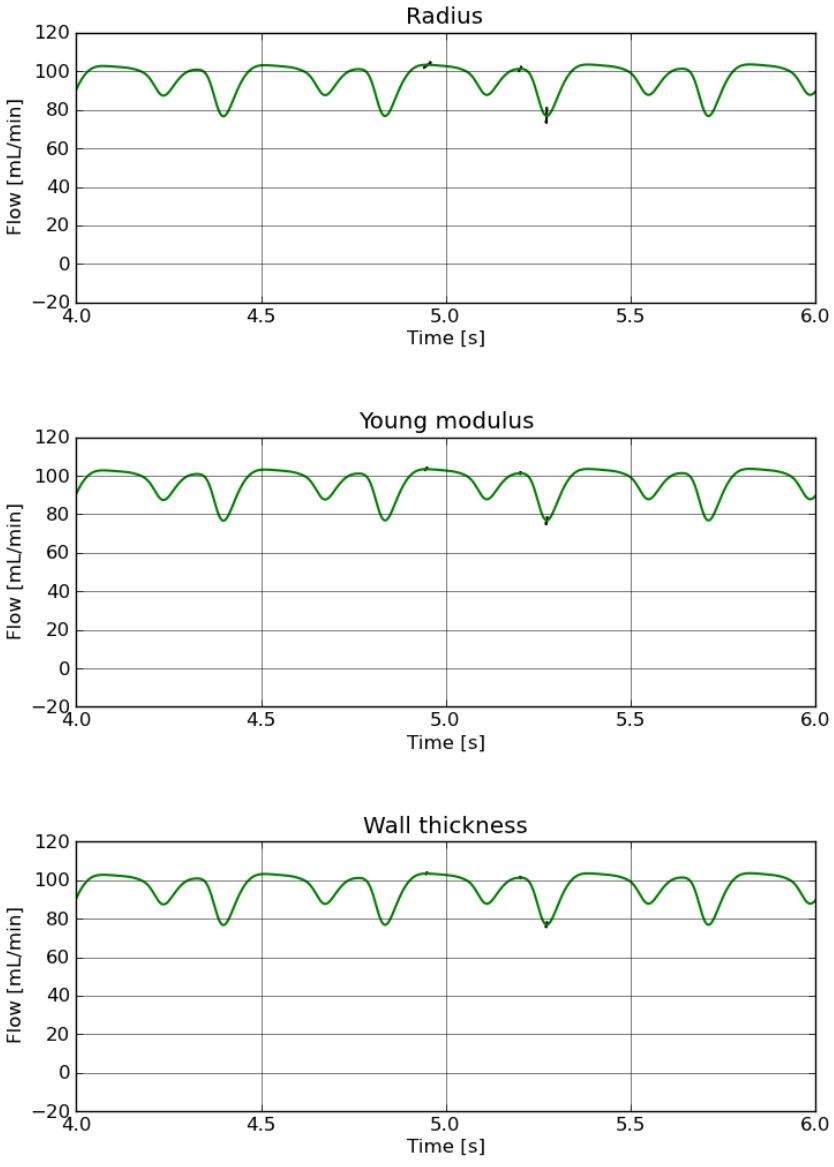

Figure 53: Sensitivity of peaks in umbilical vein

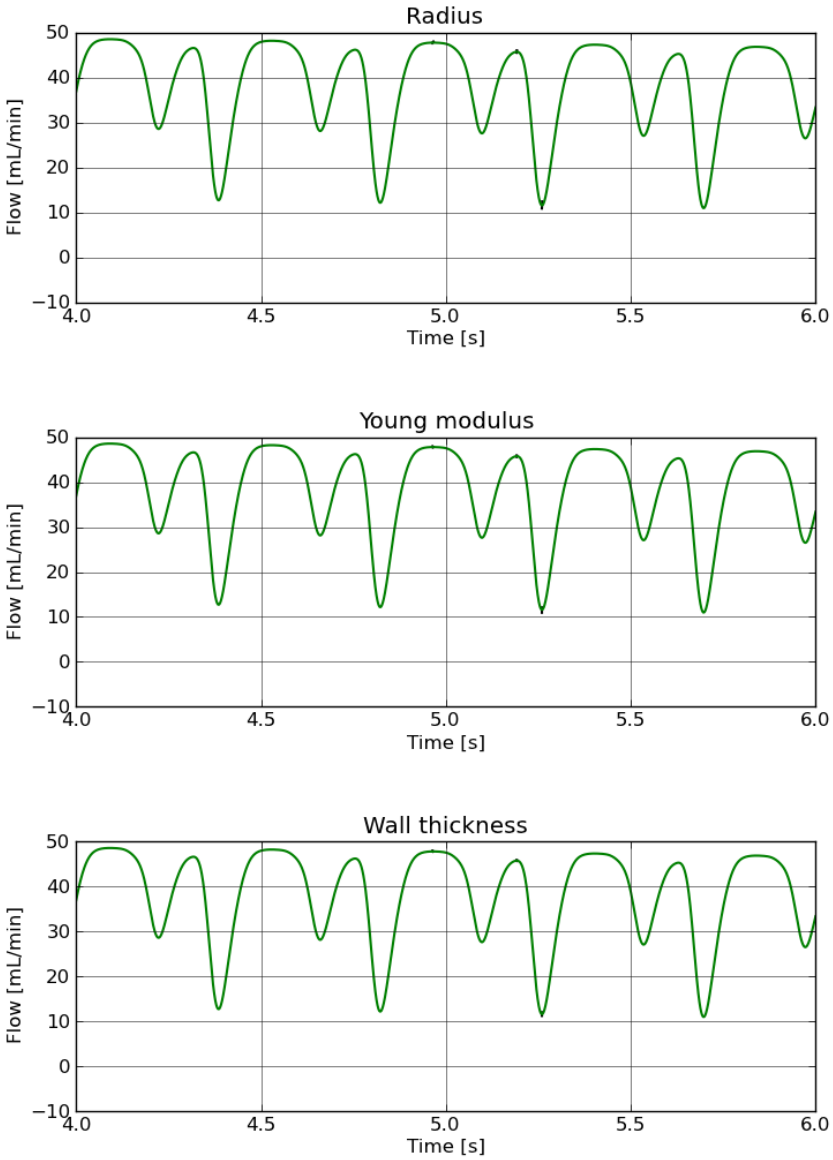

Figure 54: sensitivity of peaks in ductus venosus

Number4

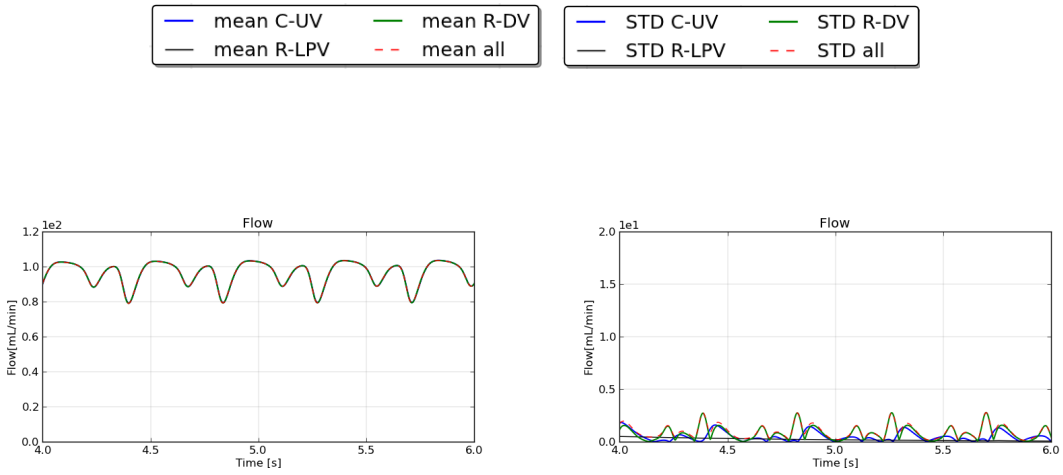

Figure 55: Total flow umbilical vein

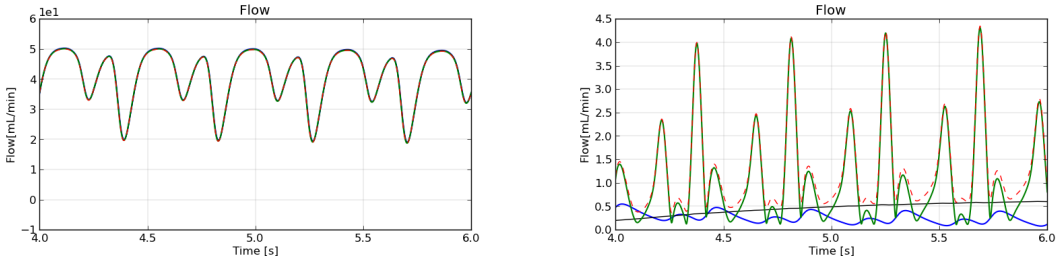

Figure 56: Total flow ductus venosus

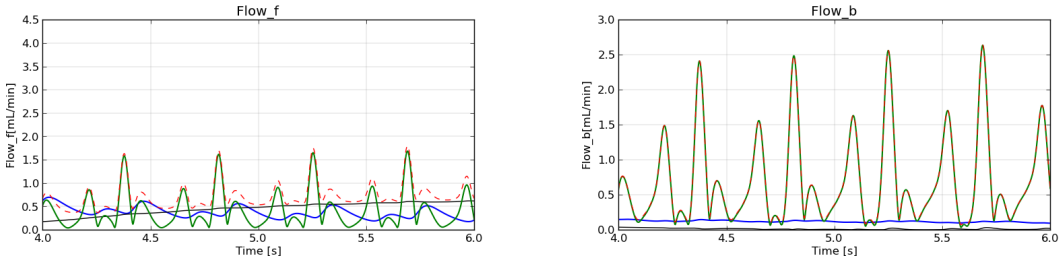

Figure 57: Left: forward flow. Right: backward flow. Both showing STD of flow in ductus venosus

Figure 55 illustrates the total flow in the umbilical vein, where both the mean and STD of the flow have been shown.The flow illustrates sensitivity due to uncertainties in parameters such as compliance and resistance. Furthermore, uncertainty in the compliance

parameter takes place at the inlet of the umbilical vein, representing the boundary condition. Moreover, an uncertainty in the resistance has been applied for both LPV and DV, where they represent the He and IVC boundary conditions. Interestingly, the uncertain parameter in LPV provides less significant results as the STD is constant in time. However, the uncertain parameter in DV shows significant results where the flow vary enormously, see figure 56. Figure 57 illustrates the flow in both forward and backward directions in DV. The uncertain parameter of compliance shows a variation in flow, meaning that the forward flow in DV is sensitive to the uncertain parameter of compliance, while the backward flow in DV is less affected.

Confidence interval of stochastic simulation with uncertainty in the LPV and DV radius

This simulation was performed in order to point out the strong impact on flow due to the radius of DV. The sensitivity of peaks are demonstrated below, see figures 58, 59 and 60. It can be observed from these figures that the flow is highly sensitive to the radius of DV in all vessels, i.e umbilical vein, left portal vein and ductus venosus. In contrast, less sensitivity is demonstrated due to an uncertainty in the radius of LPV.

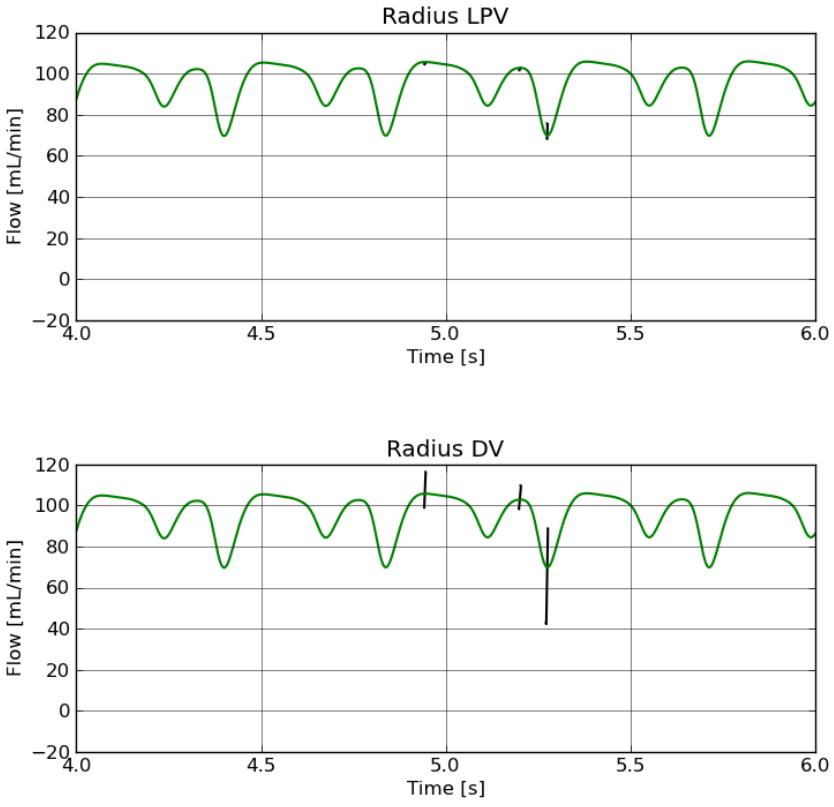

Figure 58: Sensitivity of peaks in umbilical vein

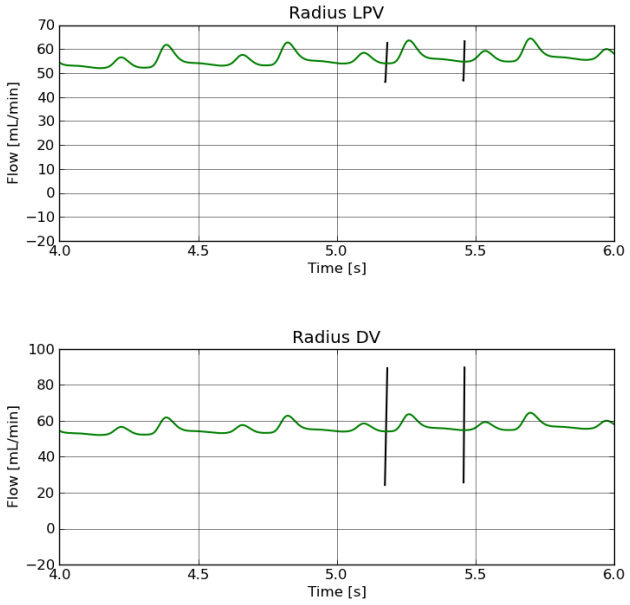

Figure 59: Sensitivity of peaks in left portal vein

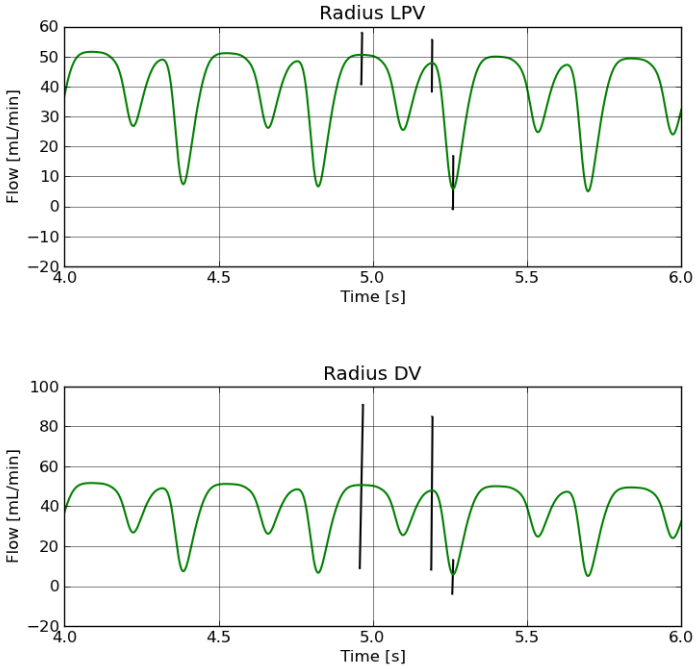

Figure 60: Sensitivity of peaks in ductus venosus

9 Discussion

The pulsatile flow in the left portal vein is a reflected image of the pulsatile flow in ductus venosus. Consequently, the a-wave occurs as a peak rather than a nadir in LPV [31]. According to the wave intensity analysis, the flow wave travelling in the opposite direction of pressure will change direction and flaps to the opposite side. The pressure gradient between umbilical vein and ductus venosus as well as the pressure gradient between the umbilical vein and left portal vein may be different, and the flow will come as a result of this. The area of interest in this thesis includes different boundary conditions, whereas the umbilical vein is the source of flow, while LPV and DV are the sources of pressure, creating a pressure difference as well as a flow-pressure interaction between the three vessels.

Pennati et al. state that it is the geometry of the umbilical vein/ ductus venosus branching, in particular, the inlet at the ductus venosus that is the major determinant of the umbilical blood flow shunting [19]. In addition, both venous pressure and the level of hematocrit were indicated as possible determinants of flow distributions due to affection of liver resistance [19]. Nevertheless, the hematocrit has not been directly investigated in this thesis, yet the resistance in the left portal vein has been adjusted, enabling us to analyse the respond in blood flow behaviour. This is demonstrated in section 8.1.2 and 8.1.4.

Furthermore, several parameters related to the fluid dynamics of the blood vessels have been adjusted. The diameter, wall thickness and young modulus represent the material properties of the vessels. Other parameters such as resistance, compliance and pressure represent the boundary conditions of the liver, inferior vena cava and the right atrium and placenta. The following questions will be discussed in this section

1. What is the case of increased shunting through DV?
2. What supports the abnormal flow in DV, i.e, reversed flow ?
3. What parameter provide high pulsations in the three vessels?
4. Which material parameter gives high uncertainty in the context of pulsations in UV and DV?
5. What supports transmitted waves into UV ?

Concerning question 1, the degree of shunting through DV was investigated in Test 1 and Test 2. It was found that the flow distribution of the left portal vein and ductus venosus altered enormously for the various cases. Test 1 in table 4 involved a high wall thickness of DV, and showed a great difference between the flow distribution of LPV and DV. The highest volume flow shunted through DV was found in case 1 where the DV inlet was set equal to 2.2 mm providing the highest DV/UV ratio. The lowest amount

of flow shunted through DV was obtained in case 3 where the DV/UV ratio was at the lowest. Moreover, the variance between the flow distributed between LPV and DV was minor in case 6, not surprising due to the small difference in geometry between LPV and DV. Interestingly, the only case creating a higher volume flow through DV rather than LPV was in case 1. Case 1 involves a relatively high diameter of DV.

Furthermore, this is also the case for Test 2, see table 5, where both the wall thickness and young modulus in DV have been decreased. When the flow through DV is higher only for case 1 in Test 1, it is higher for all cases except case 3 and 7 in Test 2. Interestingly, this demonstrates the sensitivity of flow due to the stiffness and wall thickness of the vessels. Moreover, the diameter difference is also a clear indicator of flow distribution between DV and LPV which is demonstrated by case 3 in Test 2, see table 5. Here the diameter LPV/DV ratio is high, resulting in a flow direction towards LPV. In addition, case 7 is also demonstrating a higher flow shunted through LPV, yet less markedly. The reason is due to a different diameter of UV for case 3 and 7, reflecting the flows dependency on diameter of the three vessels acting together. Accordingly, this is a result demonstrating that for a high UV diameter, the flow transmitted back into UV is high, reducing the flow through LPV.

Furthermore, the sensitivity of flow due the parameters discussed above will be further explained in context of stochastic modelling.

Concerning question 2, the parametric study in section 8.1.2 was established. It was discovered that abnormal flow occurs in DV when the pressure originated from the heart increases. The pressure difference between DV and LPV have an enormous impact on the flow distribution between the two vessels. As illustrated in figures 20 and 21 in section 8.1.2, the abnormal a-wave in ductus venosus occurs when pulsatile pressure in the lumped IVC compartment increases. It showed high response to the $P_{A,IVC}$ representing the maximum pressure amplitude, see equation 81. Reversed flow was a result and is demonstrating the reason for the often occurrence of reversed flow during atrial contraction. As discussed in section 3, the atrial contraction wave is an indicator of several fetal diseases and it is therefore important to understand the physics providing such reversed flow. Case 1,6 and 9, see figures 20 and 21, represent the highest pulsations in DV with the following reversed blood flow, where the latter is the case with the highest P_{0W} in the IVC compartment. The main reason for the flow distribution is the total pressure difference between LPV and DV, where case 1,6 and 9, represents a pressure difference of 2.6, 1.6 and 3 Pa in favour of DV respectively. Consequently, case 1,6 and 9 gives rise to the most abnormal flow in DV.

Regarding question 3, a parametric study including 7 various geometries was performed. It was discovered that the highest pulsatile flow within all vessels were obtained for case 1, see figures 23, 26 and 29. This is explained by the high DV diameter, and is supporting Kiserud T. [29] statement that it is particularly the diameter of DV that influence the pulsatility of flow.

The pulsations decreased in case 2 and further decreased in case 3, meaning that the pulsations occurring in UV, LPV and DV are dependant on the DV diameter. Accordingly, the DV/UV ratio is of high importance when investigating the pulsations in the umbilical vein in context of fetal disease. This is in accordance with Hellevik et al. [16], where it was stated that for increasing UV/DV diameter ratio, the pulsations decreased.

Less variation in pulsations is observed in case 2,6 and 7 where the LPV diameter is altered, and DV and UV diameters fixed to 1.6 and 6.1 mm respectively, see figures 25, 31 and 28. However, an observation from the figures is that the degree of shunting through LPV and DV is different, whereas a higher volume flow is shunted through DV for low LPV diameter and vice versa.

Furthermore, a variation in the diameter of UV has minor influence on the flow, see figure 24, 30 and 27. These figures illustrate the flow pattern in DV, UV and LPV where a variation in UV diameters have been applied.

This signifies that the pulsations occurring in the three vessels are mostly dependent on the diameter of DV. This is assumably due to the presence of pulsatile flow generated by the heart, transmitted into IVC and further into DV. This is in agreement with Hellevik et al. [16], where it was stated that the dimensions of the vessels do influence the pulsations in the umbilical vein. In addition, it was stated that the magnitude of the pressure and flow waves generated by the fetal heart had an impact on the pulsations in the umbilical vein.

Furthermore, the influence caused by a variation of the material parameters was also explored, yet by means of stochastic modelling, that enables a sensitivity analysis, elaborated in section 6.1, of the various model parameters.

In order to answer questions 4 and 5, stochastic modelling was employed. The sensitivity analysis was utilized in order to examine the influence on flow due to uncertainty of material parameters. The parameters giving rise to a high standard deviation within the flow pattern imply high sensitivity of the respected parameters.

Involving an uncertainty of the diameter of both the umbilical vein and the ductus venosus showed significant differences for the two vessels. The umbilical vein showed quantity standard deviation related to the uncertainty of DV diameter, yet minor influence by the uncertainty of UV itself, see figure 32. Moreover, the backward blood flow demonstrated that the pulsations only were dependent on the diameter of DV, see figure 33. However, it was also dependent on the diameter of UV, yet only by a constant value. This means that the diameter of UV does not affect the pulsatile flow pattern transmitted back into UV, but the volume transmitted. The same observations were found in the ductus venosus, only here the forward flow was of interest, see figure 35. In the context of growth restricted fetuses, it has been observed that a high degree of shunting through DV is due to high diameter of DV. In addition, a high diameter of DV also provide pulsatile flow back into UV. This has been demonstrated in Number 1.

Moreover, the uncertainty of LPV diameter does not affect the flow pattern in UV as

much as the diameter of DV. This is demonstrated in figure 58 and 60.

Another simulation was consistently aiming at which material parameter that has a great impact on flow. The same parameters as investigated before were utilized. Firstly, a sensitivity analysis concerning the parameters in ductus venosus was performed. The umbilical vein showed a remarkable difference in sensitivity. The increased DV diameter imply an increased volume flow, whereas the wall thickness and young modulus had minor influence, see figure 40. The same is observed for ductus venosus, see figure 42. Moreover, the STD of UV and DV showed high sensitivity to the flow wave during atrial contraction, yet with opposite directions. As explained before, the flow and pressure directions are decisive for the flow wave behaviour. Interestingly, the STD of the backward flow occurring in UV has the same direction as in DV, where the STD of peaks is in the negative direction with a pulsatile behaviour, see figures 41 and 42. On the contrary, the total flow in UV shows a STD increase. Thus, the results in UV and DV are in good agreement with the wave intensity analysis, discussed in section 3.3, where the flow flaps to the opposite direction when travelling in the opposite direction of pressure.

Secondly, the same material parameters were assumed to be uncertain in the umbilical vein. The umbilical vein showed the same sensitivity, as observed in Number 2, yet the pulsations in the backward flow were almost zero. This explains that the pulsations transmitted back into the umbilical vein are only due to material parameters in DV, see figure 49 and this result supports Hellevik et al. [16]. However, the ductus venosus responded differently than before. The values of the standard deviation tend to zero, showing an almost ignored response of the uncertainty in UV, see figure 50 (Note that the y-axis are different for each Number). This is also demonstrated in figures 53 and 54 where confidence intervals of the simulation are illustrated.

Consequently, from the above discussion, the flow in umbilical vein is strongly dependant on the material properties and geometry of DV. Thus, the pressure waves originating at the heart transmitting into DV are seen as the main cause of pulsatile flow in UV. Therefore, the importance of good understanding regarding the characteristic of DV is essential when examining the flow pattern in the umbilical vein.

The simulations with an uncertainty in compliance and resistance at the lumped boundary conditions such as umbilical vein, left portal vein and ductus venosus are demonstrated in figures 55 and 55. Simulations have been carried out with an uncertainty in the compliance and resistance term in the $\mathcal{L}$ and Windkessel networks, respectively. This has been done in order to present a compliant placenta and resistant liver and IVC compartments. The effect and influence on flow demonstrate the sensitivity of the different parameters. It must be stated that the flow in LPV is not presented due to difficulties in the simulation. However, the sensitivity in flow due to an uncertainty regarding the resistance in the He compartment is presented for both UV and DV. Furthermore, the most significant parameter providing high STD is the resistance parameter in the IVC compartment. This may be explained by the presence of heart. As already mentioned, a

time varying pressure takes place at this section, see equation 81 for description.

Moreover, the resistance in DV has different impact on the three vessels, where it provides high sensitivity in DV, while minor in UV. Concerning the compliant placenta, the impact is as well different regarding flow in UV and DV. Accordingly, the flow in DV is more sensitive to the compliant placenta than the flow in UV, where it tends to zero. However, figure 57 is illustrating the backward flow in DV, where the compliant placenta imply a rather constant STD in time, while forward flow include a varying STD.

The resistance in He compartment signifies a constant STD in time. However, in UV it can be neglected, while in DV it influences the flow by increasing the volume. Nevertheless, the backward flow in DV is not influenced much due to an uncertainty in the He compartment at LPV, meaning that the resistance in He only affects the flow shunted into DV in the forward direction. Moreover, the flow distribution is dependent on the difference in resistance at the He and IVC compartments, yet pulsatile flow is strongly dependant on the characteristic of DV and the IVC condition. In addition, the highest STD takes place at the wave during atrial contraction.

10 Conclusion

In conclusion, the reversed flow often observed in chromosomal abnormalities and cardiac defects are explained by the pressure difference between the left portal vein and ductus venosus, whereas a high pressure at the IVC compartment provides the most abnormal flow in DV. In addition, a high pressure difference between LPV and DV creates an even more reversed blood flow in DV. The degree of shunting through DV is increasing for a fetus affected by Hypoxia or IUGR. It has been demonstrated that the main reason for a high distribution of flow through DV is due to high DV diameter. In addition, a reduced stiffness and wall thickness in DV bring about an even more significant volume flow. Pulsations occurring in UV are mainly due to the diameter of DV, while an increasing volume flow transmitted back into UV occur due to an extended UV diameter. Stochastic modelling gives rise to a sensitivity analysis. As a result, the uncertain parameter with high influence on the flow pattern may be detected. The figures in this thesis exhibit the sensitivity of flow, where strong variation indicates high sensitivity. The parameter with the highest sensitivity is the radius of DV.

11 Suggestions for Further Work

In this current work it is the intra abdominal portion of the umbilical vein that is examined. However, the connection between the outer abdominal portion of the umbilical vein should be taken into consideration as well. Nevertheless, in the literature it is mainly the intra portion that receives attention and it is probably correct to assume that little is known about the mechanical properties of the outer abdominal portion. However, it is likely to believe that at the entrance from the outer portion of the umbilical vein is much more resistant and that an increase in compliance takes place. Moreover, the region of area is also likely to be of very small dimensions making the simulations difficult, especially when a 1D model has been applied. Therefore, it is suggested that a higher dimensional model, such as 3D is applied when investigating this particular area. Increased learning about this area will also increase the knowledge about the bifurcation that has been investigated in this thesis due to the wave propagation. What boundary condition that takes place at the terminal of each vessel will highly influence the flow, hence the boundary condition at the inlet of the intra abdominal umbilical vein will indeed affect the flow pattern at the ductus venosus and left portal vein.

A Appendix

Xml-file of the Network in Case I

```
<?xml version='1.0' encoding='ISO-8859-1'?>
<DVny.xml version="2.0" id="1.0">
  <simulationContext>
    <CFL>0.75</CFL>
    <totalTime unit="s">6.0</totalTime>
    <NumScheme>MacCormack</NumScheme>
    <EqSystem>2</EqSystem>
    <CharSystem>0</CharSystem>
  </simulationContext>
   <boundaryConditions>
 <boundaryCondition vessel_id="0">
       <Q2m>
        <Q0_m unit="ml min-1">96.7</Q0_m>
        <Tmean unit="s">0.0</Tmean>
        <Traise unit="s">1.0</Traise>
      </Q2m>
      <Lnet>
<Z unit="Pa s mm-3">None</Z>
<C unit="ml mmHg-1">0.3</C>
<C-interval unit="ml mmHg-1"></C-interval>
       </Lnet>
   </boundaryCondition>
  <boundaryCondition vessel_id="1">
       <P2m>
<P0_m unit="mmHg">4.3</P0_m>
<P0_m-interval unit="mmHg"/>
<Tmean unit="s">0.0</Tmean>
<Traise unit="s">1.0</Traise>
</P2m>
<WK3>
<Rc unit="mmHg s ml-1">0.16</Rc>
<Rc-interval unit="mmHg s ml-1"></Rc-interval>
<C unit="ml mmHg-1">3.0</C>
<C-interval unit="ml mmHg-1"/>
<Z unit="mmHg s ml-1">None</Z>
```

```
<RT unit="mmHg s ml-1">None</RT>
</WK3>
    </boundaryCondition>
    <boundaryCondition vessel_id="2">
<Fou>
<P0_m unit="mmHg">1.4</P0_m>
<P0_m-interval unit="mmHg"/>
<Tmean unit="s">0.0</Tmean>
<Traise unit="s">1.0</Traise>
<scale unit="mmHg">3.0</scale>
<scale-interval unit="mmHg"/>
<Npulse unit="">15.0</Npulse>
<Tpulse unit="s">1.0</Tpulse>
</Fou>
        <WK3>
<Rc unit="mmHg s ml-1">0.04</Rc>
<Rc-interval unit="mmHg s ml-1"></Rc-interval>
<C unit="ml mmHg-1">0.4</C>
<C-interval unit="ml mmHg-1"></C-interval>
<Z unit="mmHg s ml-1">None</Z>
<RT unit="mmHg s ml-1">None</RT>
</WK3>
    </boundaryCondition>
  </boundaryConditions>
  <globalFluid>
    <my unit="Pa s">None</my>
    <rho unit="kg m-3">1060.0</rho>
    <gamma unit="">2.0</gamma>
    <dlt unit="">1.33333333333</dlt>
    <pref unit="Pa">None</pref>
  </globalFluid>
    <vessels>
  <vessel name="UV" end_node="1" rightDaugther="1" leftDaugther="2" angleToMother="0.0
      <grid>
        <geom>Cone</geom>
        <N>
          <scalar unit="">28</scalar>
          <interval unit=""/>
        </N>
        <length>
```

```
      <scalar unit="mm">35</scalar>
      <interval unit="mm"></interval>
    </length>
    <radiusA>
      <scalar unit="mm">6.1/2</scalar>
      <interval unit="mm"></interval>
    </radiusA>
  </grid>
  <solid>
    <comp>Laplace</comp>
    <Pfunc>False</Pfunc>
    <Ps unit="Pa">133.32</Ps>
    <As unit="m2">2.74645883758e-06</As>
    <beta>
      <scalar unit="Pa m-1">None</scalar>
      <interval unit="Pa m-1"/>
    </beta>
    <wallThickness>
      <scalar unit="mm">0.61</scalar>
      <interval unit="mm"></interval>
    </wallThickness>
    <youngModulus>
      <scalar unit="Pa">17500</scalar>
      <interval unit="Pa"></interval>
    </youngModulus>
  </solid>
  <fluid>
    <my unit="Pa s">0.004</my>
    <rho unit="kg m-3">1060.0</rho>
    <gamma unit="">2.0</gamma>
    <dlt unit="">None</dlt>
    <pref unit="">0.0</pref>
  </fluid>
</vessel>
<vessel name="PV" end_node="2" rightDaugther="None" leftDaugther="None" angleToMot
  <grid>
    <geom>Uni</geom>
    <N>
      <scalar unit="">8</scalar>
      <interval unit=""/>
```

```
    </N>
    <length>
      <scalar unit="mm">7.5</scalar>
      <interval unit="mm"/>
    </length>
    <radiusA>
      <scalar unit="mm">3.5/2</scalar>
       <interval unit="mm"></interval>
    </radiusA>
  </grid>
  <solid>
    <comp>Laplace</comp>
    <Pfunc>False</Pfunc>
    <Ps unit="Pa">133.32</Ps>
    <As unit="m2">1.69716689129e-06</As>
    <beta>
      <scalar unit="Pa m-1">None</scalar>
      <interval unit="Pa m-1"/>
    </beta>
    <wallThickness>
      <scalar unit="mm">0.35</scalar>
      <interval unit="mm"/>
    </wallThickness>
    <youngModulus>
      <scalar unit="Pa">17500</scalar>
      <interval unit="Pa"/>
    </youngModulus>
  </solid>
  <fluid>
    <my unit="Pa s">0.004</my>
    <rho unit="kg m-3">1060.0</rho>
    <gamma unit="">2.0</gamma>
    <dlt unit="">None</dlt>
    <pref unit="">0.0</pref>
  </fluid>
</vessel>
<vessel name="DV" end_node="3" rightDaugther="None" leftDaugther="None" angleToMot
  <grid>
    <geom>Uni</geom>
    <N>
```

```
          <scalar unit="">10</scalar>
          <interval unit=""/>
        </N>
        <length>
          <scalar unit="mm">12.5</scalar>
          <interval unit="mm"/>
        </length>
        <radiusA>
          <scalar unit="mm">1.6/2</scalar>
          <interval unit="mm"></interval>
          </radiusA>
      </grid>
      <solid>
        <comp>Laplace</comp>
        <Pfunc>False</Pfunc>
        <Ps unit="Pa">133.32</Ps>
        <As unit="m2">6.78866756514e-06</As>
        <beta>
          <scalar unit="Pa m-1">None</scalar>
          <interval unit="Pa m-1"/>
        </beta>
        <wallThickness>
          <scalar unit="mm">0.16</scalar>
          <interval unit="mm"/>
        </wallThickness>
        <youngModulus>
          <scalar unit="Pa">10477</scalar>
          <interval unit="Pa"/>
        </youngModulus>
      </solid>
      <fluid>
        <my unit="Pa s">0.004</my>
        <rho unit="kg m-3">1060.0</rho>
        <gamma unit="">2.0</gamma>
        <dlt unit="">None</dlt>
        <pref unit="">0.0</pref>
      </fluid>
    </vessel>
  </vessels>
</DVny.xml>
```

References

[1] Bramwell J. Hill A. The velocity of the pulse wave in man. *R Soc London*, 1922.

[2] J.E. Davies A.D. Hughes, K.H.Parker. Waves in arteries: A review of wave intensity analysis in the systemic and coronary circulations. *Artery Research*, 2(2):51 – 59, 2008.

[3] Gasperi C Battaglia F Ferrazzi E Bellotti M, Pennati G. Role of ductus venosus in distribution of umbilical blood flow in human fetuses during second half og pregnancy. Technical report, 2000.

[4] Xiu D. Fast numerical methods for stochastic computations. Technical report, 2009.

[5] F.Vosse D.Bessems, M. Rutten. A wave propagation model of blood flow in large vessels using an approximate velocity profile function. *Jorunal of Fluid Mechanics*, 580:145–168, 2007.

[6] Ream M. Ray A.M. Chandra Rashmi. Chikaraishi D.M. Early fetal hypoxia leads to growth restriction and myocardial thinning. *Am J Physiol Regul Integr Comp Physiol*, 295:583 – 595, 2008.

[7] Bellotti M. Pennati G. Gasperi CD. Bozzo M. Battaglia FC. Ferrazzi E. Simultaneous measurements of umbilical venous, fetal hepatic, and ductus venosus blood flow in growth-restricted human fetuses. Technical report, 2004.

[8] N.Stergiopulos F. N. Vosse. Pulse wave propagation in the arterial tree. 2011.

[9] D.Faber M.Ramsay N.Westerhof M.Gemert J.Winjgaard, B.Westerhod. Abnormal arterial flows by a distributed model of the fetal circulation. *American journal of physiology*, 291(5), 2006.

[10] Tchirikov M. Schroder H.J Hecher K. Ductus venosus shunting in the fetal venous circulation: regulatory mechanism, diagnostic methods and medical importance. *Ultrasound Obstet Gynecol*, 27:452 – 461, 2006.

[11] Maiz N. Valencia C. Emmanuel EE. Staboulidou I. Nicolaides KH. Screening for adverse pregnancy outcome by ductus venosus doppler at 11-13+6 weeks of gestation. Technical report, Obstet Gynecol, 2008.

[12] Matias A. Gomes C. Flack N. Montenegro N. Nicolaides K.H. Screening for chromosomal abnormalities at 10-14 weeks: the role of ductus venosus blood flow. *Ultrasound Obstet Gynecol*, 12:380–384, 1998.

[13] A.Veneziani L.Formaggia, A.Quarteroni. *Cardiovascular Mathematics*. Springer, 2009.

[14] Hellevik L.R. Biomechanic compendium.

[15] Leinan P.R. Degroote J. Kiserud T. Skallerud B. Vierendeels J. Hellevik L.R. Fluid structure interaction at the umbilical vein-ductus venousus bifurcation. Technical report, 2012.

[16] T Kiserud S.I Rabben S.H Eik-Nes F. Irgens L.R Hellevik, N Stergiopulos. A mathematical model of umbilical venous pulsation. *Journal of Biomechanics*, 33(9):1123 – 1130, 2000.

[17] F.Irgens N.Stergiopulos M.Hanson L.R.Hellevik, T. Kiserud. Mechanical properties of the fetal ductus venousus and umbilical vein. *Heart and Vessel*, pages 175–180, 1998.

[18] Haugen G. Kiserud T. Godfrey K. Crozier S. Hanson M. Portal and umbilical venous blood supply to the liver in the human fetus near term. Technical report, Ultrasound Obstet Gynecol, 2004.

[19] Pennati G. Corno C. Costantino M.L Bellotti M. Umbilical flow distribution to the liver and the ductus venosus in human fetuses during gestation. *Medical Engineering Physics*, 25:229–238, 2003.

[20] G.Pardi R.Fumero M.Bellotti, G.Pennati. Filation of the ductus venosus in human fetuses: Ultrasonic evidence and mathematical modelling. *Am J Physiol Heart Circ Physiol*, 275, 1998.

[21] O'Rourke M.J Hartley C McDonald D.A, Nichols W. *McDonalds Blood Flow in Arteries, Theoretical, experimental and clinical principles*. Arnold, 4 edition, 1998.

[22] Henry L. Galan MD. Timing delivery of the growth-restricted fetus. *Seminars in Perinatology*, 35:262–269, 2011.

[23] Matias A. Montenegro N. Ductus venosus: A love story of 14 years. Technical report, 2011.

[24] Lankhaar B. E. Westerhof Ni.Westerhof, J.W. The arterial windkessel. *Med Biol Eng Comput*, 2009.

[25] Hecher K. Campbell S. Characteristics of fetal venous blood flow under normal circumstances and during fetal disease. Technical report, 1996.

[26] Kiserud T. Kessler J. Ebbing C. Rasmussen S. Ductus venosus shunting in growth-restricted fetuses and the effect of umbilical circulatory compromise. Technical report, 2006.

[27] S.J. Sherwin, V. Franke, J. Peiró, and K. Parker. One-dimensional modelling of a vascular network in space-time variables. *Journal of Engineering Mathematics*, 47:217–250, 2003. 10.1023/B:ENGI.0000007979.32871.e2.

[28] Xiu D. Sherwin S.J. Parametric uncertaity analysisof pulse wave propagation in a model of a human arterial network. *Journal of computational physics*, 226:1385 – 1407, 2007.

[29] Kiserud T. Hemodynamics of the ductus venosus. Technical report, Unit of Fetal Medicine, Department of Obsterics and Gynecology, 1999.

[30] Kiserud T. The ductus venosus. Technical report, 2001.

[31] Kiserud T. *Doppler ultrasound in obstetrics and gynecology*. SpringerLink, 2005.

[32] Kiserud T. Physiology of the fetal circulation. *Seminars in Fetal Neonatal Medicine*, 10:493 – 503, 2005.

[33] L.R.Hellevik T.Kiserud, O .Kilavuz. Venous pulsation in the fetal left portal branch: the effect of pulse and flow direction. *Ultrasound Obstet Gynecol*, 21:359–364, 2003.

[34] J.J. Wang and K.H. Parker. Wave propagation in a model of the arterial circulation. *Journal of Biomechanics*, 37(4):457 – 470, 2004.

[35] R.Hose Y.Shi, P.Lawford. Zero-d and 1-d models of blood flow in the cardiovascular system. *BioMedical Engineering OnLine*, 10(1), 2011.